

Direct Imaging discovery of a second planet candidate around the possibly transiting planet host CVSO 30 [★]

T. O. B. Schmidt^{1,2}, R. Neuhauser², C. Briceño³, N. Vogt⁴, St. Raetz⁵, A. Seifahrt⁶, C. Ginski⁷, M. Mugrauer², S. Buder^{2,8}, C. Adam², P. Hauschildt¹, S. Witte¹, Ch. Hellings⁹, and J. H. M. M. Schmitt¹

¹ Hamburger Sternwarte, Gojenbergsweg 112, 21029 Hamburg, Germany, e-mail: tschmidt@hs.uni-hamburg.de

² Astrophysikalisches Institut und Universitäts-Sternwarte, Universität Jena, Schillergäßchen 2-3, 07745 Jena, Germany

³ Cerro Tololo Inter-American Observatory CTIO/AURA/NOAO, Colina El Pino s/n. Casilla 603, 1700000 La Serena, Chile

⁴ Instituto de Física y Astronomía, Universidad de Valparaíso, Avenida Gran Bretaña 1111, 2340000 Valparaíso, Chile

⁵ European Space Agency ESA, ESTEC, SRE-S, Keplerlaan 1, NL-2201 AZ Noordwijk, the Netherlands

⁶ Department of Astronomy and Astrophysics, University of Chicago, 5640 S. Ellis Ave., Chicago, IL 60637, USA

⁷ Sterrewacht Leiden, PO Box 9513, Niels Bohrweg 2, NL-2300RA Leiden, the Netherlands

⁸ Max-Planck-Institute for Astronomy, Königstuhl 17, 69117 Heidelberg, Germany

⁹ School of Physics and Astronomy SUPA, University of St. Andrews, North Haugh, St. Andrews, KY16 9SS, UK

Received 2015; accepted

ABSTRACT

Context. Direct Imaging has developed into a very successful technique for the detection of exoplanets in wide orbits, especially around young stars. Directly imaged planets can both be followed astrometrically on their orbits and observed spectroscopically, and thus provide an essential tool for our understanding of the early Solar System.

Aims. We surveyed the 25 Ori association for Direct Imaging companions, having an age of only few million years. Among other targets CVSO 30 was observed, recently identified as the first T Tauri star found to host a transiting planet candidate.

Methods. We report on photometric and spectroscopic high contrast observations with the Very Large Telescope, the Keck telescopes and the Calar Alto observatory that reveal a directly imaged planet candidate close to the young M3 star CVSO 30.

Results. The JHK-band photometry of the newly identified candidate is better than 1σ consistent with late type giants, early T and M dwarfs as well as free-floating planets, other hypotheses like e.g. galaxies can be excluded by more than 3.5σ . A lucky imaging z' photometric detection limit $z' = 20.5$ mag excludes early M dwarfs and results in less than $10 M_{\text{Jup}}$ for CVSO 30 c if bound. We present spectroscopic observations of the wide companion, implying that the only remaining explanation for the object is being the first very young (< 10 Myr) L–T type planet bound to a star, i.e. appearing bluer than expected due to a decreasing cloud opacity at low effective temperatures. All except a planetary spectral model are inconsistent with the spectroscopy, and we deduce a best mass of 4–5 Jupiter masses (total range 0.6–10.2 Jupiter masses).

Conclusions. Therefore CVSO 30 is the first system, in which both a close-in and a wide planet candidate are found to have a common host star. The orbits of the two possible planets could not be more different, having orbital periods of 10.76 hours and about 27000 years. Both orbits may have formed during a mutual catastrophic event of planet-planet scattering.

Key words. stars: pre-main sequence, low-mass, planetary systems - planets: detection, atmospheres, formation

1. Introduction

Since the first definitive detection of a planet around another main-sequence star, 51 Peg (Mayor & Queloz 1995), by high-precision radial velocity measurements, various detection techniques have been applied to find a diverse population of exoplanets. Among them the transit method, first used for HD 209458 (Charbonneau et al. 2000), later allowed for a boost of exoplanet discoveries after the successful launch of two dedicated satellite missions, CoRoT (Baglin et al. 2007) and Kepler (Koch et al. 2010; Borucki et al. 2010). Both these methods indirectly discern the presence of a planet by the influence on its host star and are most sensitive to small and moderate planet-star-separations around old, hence rather inactive main-sequence stars. The sensitivity diminishes fast for separations beyond 5 au, because as

the orbital period increases transits become less likely and the radial velocity amplitude declines. In contrast, direct imaging allows to discover planets in wide orbits around nearby pre-main sequence stars, because such young planets are still bright at infrared wavelengths as a result of the gravitational contraction during their still ongoing formation process.

Starting in 2005, when the first four co-moving planetary candidates around the solar-like stars DH Tau (Itoh et al. 2005), GQ Lup (Neuhauser et al. 2005), and AB Pic (Chauvin et al. 2005c), all with masses near the threshold of $13 M_{\text{Jup}}$ dividing brown dwarfs from planets according to the current IAU working definition, and the planet candidate around the brown dwarf 2M1207 (Chauvin et al. 2005a), were found, the total number of imaged planet candidates has now increased to about 50–60 objects. A summary can be found in Neuhauser & Schmidt (2012) and the current status is always available in several online encyclopaediae, such as the Extrasolar Planets Encyclopaedia at www.exoplanet.eu (Schneider et al. 2011). As in-situ formation at ~ 100 au to a few hundreds of au separation seems unlikely

[★] Based on observations made with ESO Telescopes at the La Silla Paranal Observatory under programme IDs 090.C-0448(A), 290.C-5018(B), 092.C-0488(A) and at the Centro Astronómico Hispano-Alemán in programme H15-2.2-002.

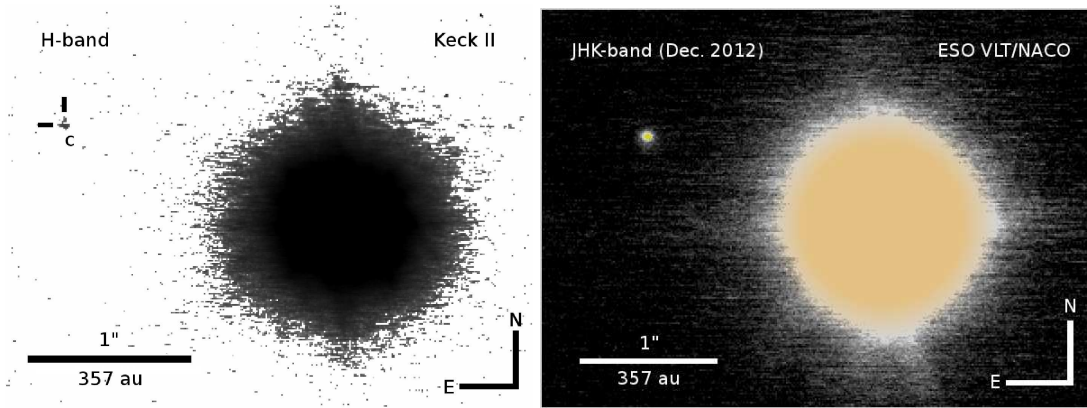


Fig. 1. Direct Images of CVSO 30 c. *Left:* Keck image of data by van Eyken et al. (2012), re-reduced. Note, the companion is Northeast, not a contaminant Southeast as given in van Eyken et al. (2012). *Right:* Our new VLT epoch, clearly showing the planetary companion, having similar color as its host star (Fig. 2), excluding it as false positive for the inner planet candidate CVSO 30 b.

according to models, Boss (2006) argue that a third body must exist, that tossed these planets outward to their present distance from their young host stars. An alternative explanation could be a stellar encounter (Adams & Laughlin 2001).

While early-type stars have less favorable planet-to-star contrast ratios, increasing evidence was found by millimeter-continuum measurements for larger and more massive protoplanetary disks, being available for planet formation around these stars (Mannings & Sargent 1997; Andrews et al. 2013). These conclusions were further strengthened as in 2008 and 2009 three of the most prominent planet candidates were found around the early F-type star HR 8799 (Marois et al. 2008), the first system with multiple planets imaged around a star, and the A-type stars Fomalhaut (Kalas et al. 2008), the first planet candidate discovered in the optical regime using the Hubble Space Telescope (HST) and β Pic (Lagrange et al. 2009, 2010), a planet within the large edge-on disk at only about twice the separation of Jupiter from the Sun, as e.g. previously predicted by Freistetter et al. (2007) from the structural gaps in the disk.

Most of the direct imaging surveys conducted so far have concentrated on AFGK stars. In 2012 a (proto)planet candidate was discovered around the ~ 2 Myr young sun-like star LkCa 15 (Kraus & Ireland 2012), a close (~ 11 AU) object found by single dish interferometry, a technique also referred to as sparse aperture masking. Recently two companions of $4\text{-}5 M_{\text{Jup}}$ were discovered around GJ 504 (Kuzuhara et al. 2013), a 160 Myrs old sun-like star and around HD 95086 (Rameau et al. 2013), an A-type star at about 10-17 Myrs. Additionally, over the past two years first results from imaging surveys around M dwarfs were published, increasing our understanding of planetary systems around the most numerous stars in the Milky Way (Delorme et al. 2013; Bowler et al. 2015).

In this article we describe for the first time the direct detection of a wide separation ($1.85''$ or 660 au, see Fig. 1) directly imaged planet candidate around a star (CVSO 30) which also hosts a short period transiting planet candidate; we refer to a more detailed discussion of this object in van Eyken et al. (2012), Barnes et al. (2013) and Yu et al. (2015). A system which harbors two planets with such extreme orbits gives us the opportunity to study the possible outcome of planet-planet scattering theories, used to explain the existence of close-in hot Jupiters in 1996 (Rasio & Ford 1996), for the first time by observations.

Table 1. Previously known CVSO 30 system data

CVSO 30	
Altern. designations	2MASS J05250755+0134243, PTF1 J052507.55+013424.3
Location	25 Ori / Orion OB 1a [1,2]
RA, Dec	05h 25m 07.57s, +01° 34' 24.5" [2]
Spectral type	M3 (weak-line T-Tauri, WTTS) [2]
Mass	0.34 / 0.44 M_{\odot} [2]
Luminosity	0.25 L_{\odot} [2]
Radius	1.39 R_{\odot} / $1.07 \pm 0.10 R_{\odot}$ / $[1.03 / 1.04 \pm 0.01 R_{\odot}]$ [2,3,4]
Temperature	3470 K [2]
Opt. extinction	0.12 mag [2]
Distance	$[323^{+233}_{-96}, 322^{+504}_{-122}]$ pc / 357 ± 52 pc [2,5]
Age	$2.39^{+3.41}_{-2.05}$ Myr [2,here]
H α equivalent width	-11.40 Å [2]
LiI equivalent width	0.40 Å [2]
$v \sin(i)_*$	80.6 ± 8.1 km s $^{-1}$ [3]
Proper Motion [E,N]	$[-0.1 \pm 5.3, 0.9 \pm 5.5]$ mas/yr [6]
B, V, R photometry	[18.35, 16.26, 15.19] mag [7,2,3]
J, H, K photometry	$[12.232 \pm 0.028, 11.559 \pm 0.026, 11.357 \pm 0.021]$ mag [8]
CVSO 30 b / PTF0 8-8695 b	
(Projected) separation	0.00838 ± 0.00072 au [3]
Period (circular)	0.448413 ± 0.000040 d [3]
Orbit. inclination	$61.8 \pm 3.7^\circ$ [3]
Orbit. misalignment	$69 \pm 2^\circ / 73.1 \pm 0.5^\circ$ [4]

References: [1] Briceño et al. (2007a), [2] Briceño et al. (2005), [3] van Eyken et al. (2012), [4] Barnes et al. (2013), [5] Downes et al. (2014) [6] Zacharias et al. (2013), [7] Zacharias et al. (2004), [8] Cutri et al. (2003); Skrutskie et al. (2006)

Table 2. CVSO 30 astrometry and photometry

	CVSO 30 b / PTFO 8-8695 b	CVSO 30 c
Separation w.r.t. the host star [E,N]		
2010 September 25		$[175.453, 63.395]$ pixel
2012 December 3		$[1.736 \pm 0.024,$ $0.638 \pm 0.009]''$
(Projected) separation	0.00838 ± 0.00072 au [1]	660 ± 131 au
Period (circular)	0.448413 ± 0.000040 d [1]	~ 27100 years
Orbit. inclination	$61.8 \pm 3.7^\circ$ [1]	
Orbit. misalignment	$69 \pm 2^\circ / 73.1 \pm 0.5^\circ$ [2]	
z' band (differential)		> 6.8 mag
J band (differential)		7.385 ± 0.045 mag
H band (differential)		7.243 ± 0.014 mag
Ks band (differential)		7.351 ± 0.022 mag
J band (differential)		7.183 ± 0.035 mag

References: [1] van Eyken et al. (2012), [2] Barnes et al. (2013)

2. 25 Ori group and the CVSO 30 system properties

Despite their importance for the evolution of protoplanetary disks and the early phases in the planet formation process, suf-

Table 4. VLT/NACO, VLT/SINFONI, archival KeckII/NIRC2 and Calar Alto/2.2m/AstraLux observation log

Instrument	JD-2455000 [days]	Date of observation	DIT [s]	NDIT	# images	Airmass	DIMM ^a Seeing	τ_0^b [ms]	Strehl [%]	S/N (brightest pixel)
NACO J	1264.69416	03 Dec 2012	15	4	15	1.13	0.8	3.7	3.2	5.9
NACO H	1264.70764	03 Dec 2012	15	4	15	1.12	0.6	4.6	11.2	24.6
NACO Ks	1264.72079	03 Dec 2012	15	4	15	1.11	0.7	4.6	23.7	11.1
NACO J	1266.72899	05 Dec 2012	30	2	15	1.12	1.3	2.8	2.0	6.6
SINFONI H+K	1592.82609	27 Oct 2013	300	2	3	1.12	0.5	5.0		$\lesssim 15$
NIRC2 H	465.05374	25 Sep 2010	3	10	12	1.25	0.4		7.0	7.8
AstraLux z'	2260.6696	26 Aug 2015	0.02945	1	70000	1.73	1.1		no AO	non-detection

Remarks: (a) Differential image motion monitor (DIMM) Seeing average of all images (b) coherence time of atmospheric fluctuations.

Table 3. CVSO 30 deduced planetary properties

	CVSO 30 b/ PTFO 8-8695 b	CVSO 30 c
Opt. extinction		$0.19^{+0.31}_{-0.19}$ mag
Luminosity (vs. \odot)		$-3.78^{+0.33}_{-0.13}$ dex
Eff. temperature T_{eff}		1600^{+120}_{-300} K
Surface gravity $\log g$		$3.6^{+1.4}_{-0.6}$ dex
Radius	$1.91 \pm 0.21 R_{\text{Jup}}$ [1] $1.64 / 1.68 \pm 0.07 R_{\text{Jup}}$ [2]	$1.63^{+0.87}_{-0.34} R_{\text{Jup}}$
Mass	$< 5.5 \pm 1.4 M_{\text{Jup}}$ [1] $3.0 \pm 0.2 M_{\text{Jup}}$ [2] $3.6 \pm 0.3 M_{\text{Jup}}$ [2]	$4.3^{+4.9}_{-3.7} M_{\text{Jup}}$ (log g & Roche) $4.7^{+5.5}_{-2.0} M_{\text{Jup}}$ (L, age) $4.7^{+3.6}_{-2.0} M_{\text{Jup}}$ (L, T_{eff} , age) $< 10 M_{\text{Jup}}$ (z' imaging limit)

References: [1] van Eyken et al. (2012), [2] Barnes et al. (2013)

ficiently large samples of 10 Myr old stars have been difficult to identify, mainly because the parent molecular clouds dissipate after a few Myr and no longer serve as markers of these populations (see Briceño et al. (2007b) and references therein). The 25 Ori cluster (“25 Ori”, Briceño et al. 2007a), contains > 200 PMS stars in the mass range $0.1 < M/M_{\odot} < 3$. The Hipparcos OB and earlier A-type stars in 25 Ori are on the zero-age main sequence (ZAMS, Hernández et al. 2005), implying a distance of ~ 330 pc, with some of the A-type stars harboring debris disks (Hernández et al. 2006). Isochrone fitting of the low mass stars yields an age of 7-10 Myr (Briceño et al. 2007b). This is the most populous 10 Myr old sample within 500 pc, which we consequently chose for a direct imaging survey with ESO’s VLT, the Very Large Telescope of the European Southern Observatory to find young planetary and sub-stellar companions at or shortly after their formation. For this same reason the 25 Ori cluster was also targeted in searches for transiting planets, like the Young Exoplanet Transit Initiative (YETI, Neuhäuser et al. 2011) and the Palomar Transient Factory (PTF, van Eyken et al. 2012).

CVSO 30 (also 2MASS J05250755+0134243 & PTFO 8-8695) is a weak-line T Tauri star of spectral type M3 in 25 Ori at an average distance of 357 ± 52 pc (Downes et al. 2014). It was confirmed as a T Tauri member of the 25 Ori cluster by the CIDA Variability Survey of Orion (CVSO), with properties shown in Table 1. As shown in Fig. 1 in van Eyken et al. (2012), CVSO 30 is one of the youngest objects within 25 Ori, its position in the color-magnitude diagram corresponding to $2.39^{+3.41}_{-2.05}$ Myr (if compared to Siess et al. (2000) evolutionary models). The object is highly variable, fast rotating and has a mass of $0.34 - 0.44 M_{\odot}$ (depending on evolutionary model) and an effective temperature of ~ 3470 K. The rotation period of CVSO 30, possibly synchronized with the CVSO 30 b orbital period, is still debated (van

Table 5. Astrometric calibration of VLT/NACO

Object	JD - 2456000 [days]	Pixel scale [mas/pixel]	PA ^a [deg]
47 Tuc	264.62525	13.24 ± 0.05	$+0.6 \pm 0.5$

Remarks: All data from Ks-band images. (a) PA is measured from N over E to S.

Eyken et al. 2012; Koen 2015). Kamiaka et al. (2015) conclude the stellar spin period to be less than 0.671 d.

In 2012 the PTF team (van Eyken et al. 2012) reported a young transiting planet candidate around CVSO 30, named PTFO 8-8695 b, with a fast co-rotating or near co-rotating 0.448413 day orbit. The very same object, henceforth CVSO 30 b for simplicity, was independently detected with smaller telescopes within the YETI (Neuhäuser et al. 2013; Errmann et al. 2014), confirming the presence of the transit events by quasi-simultaneous observations.

Keck and Hobby-Eberly Telescope (HET) spectra (van Eyken et al. 2012) set an upper limit to the mass of the transiting companion of $5.5 \pm 1.4 M_{\text{Jup}}$ from the radial velocity variation, which exhibits a phase offset likely caused by spots on the surface of the star. This RV limit was already corrected for the derived orbital inclination $61.8 \pm 3.7^\circ$ of the system. With an orbital radius of only about twice the stellar radius and a planetary radius of $1.91 \pm 0.21 R_{\text{Jup}}$, the object appears to be at or within its Roche limiting orbit, raising the possibility of past or ongoing mass loss. A false positive by a blended eclipsing binary is unlikely, as the only present contaminant in Keck near-IR images (see Fig. 1) with 6.96 mag of contrast to the star would have to be very blue to be bright enough in the optical to mimic a transit, unlikely to be a star in that case.

In 2013 Barnes et al. (2013) fit the two separate lightcurves observed in 2009 and 2010, which exhibited unusual differing shapes, simultaneously and self-consistently with planetary masses of the companion of $3.0 - 3.6 M_{\text{Jup}}$. They assumed transits across an oblate, gravity-darkened stellar disk and precession of the planetary orbit’s ascending node. The fits show a high degree of spin-orbit misalignment of about 70° , which leads to the prediction that transits should disappear for months at a time during the precession period of this system. The lower planet radius result of $\sim 1.65 R_{\text{Jup}}$ is consistent with a young, hydrogen-dominated planet that results from “hot-start” formation mechanisms (Barnes et al. 2013).

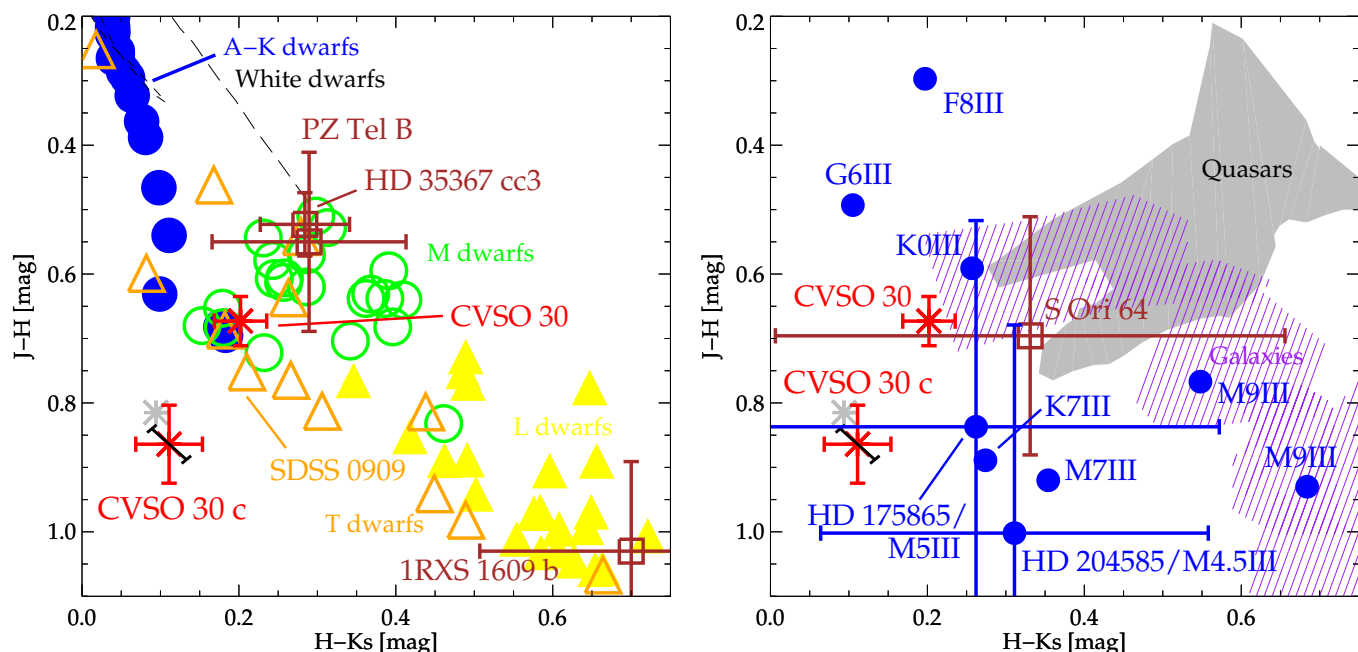


Fig. 2. CVSO 30, CVSO 30 c and comparison objects, superimposed onto the color data from Hewett et al. (2006). CVSO 30 c clearly stands out in the lower left corner, approximately consistent with colors of giants, early M and T dwarfs and free-floating planetary mass objects (Zapatero Osorio et al. 2000; Peña Ramírez et al. 2012), e.g. consistent with absolute magnitude and J-Ks color of S Ori 64. Its unusual blue color can most likely be attributed to the youth of such objects (Saumon & Marley 2008), leading to L–T transition opacity drop at high brightnesses (see Fig. 11). See Fig. A.5 for details. For CVSO 30 c we give the colors before (gray) and after (red) correction from the NACO to the 2MASS filter set as well as maximum possible systematic photometric offsets caused by variability of the primary star used as reference (black).

3. Astrometric and photometric analysis

After the discovery of the transiting planet candidate by van Eyken et al. (2012) and our independent detection of the transit signals with YETI, we included the system in our 25 Ori VLT/NACO direct imaging survey with the intent to prove that the object labeled as a contaminant by van Eyken et al. (2012) is not able to produce the detected transiting signal and to confirm it as second planet. We performed our first high resolution direct observations in December 2012 and obtained JHK-band photometry (Tables 2 & 4, Fig. 1).

During the course of their study of the transiting planet CVSO 30 b the PTF team used Keck II/NIRC2 H-band images obtained in 2010 to identify contaminants capable of creating a false positive signal mimicking a planet. We re-reduced these data, and found it already contains the planetary companion CVSO 30 c, that we report here. In Fig. 1 we show the companion, erroneously given to lie Southeast in van Eyken et al. (2012), actually being Northeast of the host star CVSO 30.

After astrometric calibration of the VLT/NACO detector epoch using a sub-field of 47 Tuc (Table 5) to determine pixel scale and detector orientation in order to find precise values for the separation of CVSO 30 c with respect to CVSO 30 in right ascension and declination, we find the object to be $\sim 1.85''$ NE of CVSO 30 at a position angle of $\sim 70^\circ$ from North towards East, corresponding to a projected separation of 660 ± 131 au at the distance of the star. Although no astrometric calibrator could be found in the night of the Keck observations (hence the position of the object is given in pixels in Table 2), we note that using the nominal pixel scale of NIRC2 of $0.009942''/\text{pixel}$ ($\pm 0.00005''$) and assuming 0° detector orientation the Keck epoch, resulting in 1.744 arcsec right ascension and 0.630 arcsec declination separation in the relative position of CVSO 30 c with respect to its host star is consistent with the VLT data. This was expected for

a companion as the proper motion of CVSO 30 is too small to distinguish a background source from a sub-stellar companion based on common proper motion (Table 1).

CVSO 30 is in general currently not suitable for a common proper motion analysis, as the errors in proper motion exceed the proper motion values (Table 1). As orbital motion around the host star might be detectable, we performed a dedicated orbit estimation for the wide companion. The analysis shows that even after 2-3 years of epoch difference no significant orbital motion is expected for the wide companion (Fig. A.1).

Using the Two Micron All Sky Survey (2MASS) (Cutri et al. 2003; Skrutskie et al. 2006) photometry for the primary and our NACO images for differential brightness measurements, we find CVSO 30 c to exhibit an unusually blue H-Ks color, while its J-H color indicates the companion candidate to be redder than the primary. This implies, that the companion is too red to be an eclipsing background binary mimicking the transiting signal of CVSO 30 as a false positive signal, which is further indication for the planetary nature of CVSO 30 b.

The differential photometry (Table 2) of CVSO 30 c was achieved using psf fitting with the *Starfinder* package of IDL (Diolaiti et al. 2000) using the primary star CVSO 30 as psf reference. First the noise of the final jittered image was computed, taking the photon noise, the gain and RON as well as the number of combined images into account, and then handed to the starfinder routine for psf fitting, resulting in the values given in Table 2. The values were checked with aperture photometry.

As given in van Eyken et al. (2012) our psf reference CVSO 30 varies by 0.17 mag (min to max) in the R band, consistent with our estimates within YETI. As a present steep wavelength dependence of the variability amplitudes is best described by hot star-spots (Koen 2015), we can extrapolate from measurements of the very similar T Tauri GQ Lup (Broeg et al. 2007), that 0.17

mag in R correspond to about 0.1 mag and 0.055 mag variability in J and Ks band respectively. As the hot spots change the bands simultaneously this gives rise to a maximum systematic offset of 0.045 mag in J-Ks color. We give an estimate of this variability as black error bars for a possible additional systematic offset of CVSO 30 c in Fig. 2.

The colors of CVSO 30 and CVSO 30 c are very similar (Table 2 & Fig. 2). As we do not have a spectrum of CVSO 30 c in J band, yet, we use the M3V star Gl 388 (Cushing et al. 2005; Rayner et al. 2009) and the L3/L4 Brown Dwarf 2MASS J11463449+2230527 (Cushing et al. 2005) to derive a preliminary filter correction between 2MASS and NACO for CVSO 30 and CVSO 30 c. The colors of CVSO 30 are well known from 2MASS (Table 1), the differential brightnesses to CVSO 30 c vary from NACO to 2MASS by 28 mmag in J, -21 mmag in H and -38 mmag in Ks. Thus CVSO 30 c is 49 mmag redder in J-H and 17 mmag redder in H-Ks in 2MASS (red in Fig. 2) compared to the NACO results (gray in Fig. 2).

In Fig. 2 and Table 6 we compare CVSO 30 c to the colors of several possible sources. We find that background stars of spectral types OBAFGK are too blue in J-H, late M dwarfs are too blue in J-H and too red in H-K, while foreground L- and late T-dwarfs are either too red in H-K or too blue in J-H. In addition, background galaxies, quasars and H/He white dwarfs are also inconsistent with the values of CVSO 30 c. Only late type giants, early M- and T-dwarfs and planetary mass free-floating objects, e.g. found in the σ Orionis Star Cluster have comparable colors (Zapatero Osorio et al. 2000; Peña Ramírez et al. 2012).

4. CVSO 30 c spectroscopic analysis

As a common proper motion analysis is not feasible because of the low proper motion of the host star (Table 1), we carried out spectroscopic follow-up observations at the end of 2013, using the ESO VLT integral field unit SINFONI. The observations were done in H+K band with 0.1 mas/spaxel scale (FoV: 3 arcsec x 3 arcsec). The instrument provides us with information in the two spatial directions of the sky in addition to the simultaneous H- and K-band spectra. An unfortunate timing of the observations led to a parallactic angle at which a spike, likely of the telescope secondary mounting was superimposed onto the well separated spectrum of the companion candidate CVSO 30 c.

After correction the resulting spectrum can be compared to model atmospheres to determine its basic properties and to other sub-stellar companions to assess its youth and the reliability of the models at this low age, surface gravity and temperature regime.

In an attempt to optimally subtract the spike of the host star we performed several standard and customized reduction steps. After dark subtraction, flatfielding, wavelength calibration and cube reconstruction, we found that the spike was superimposed onto the companion in every one of the 3 individual exposures, however at slightly different orientation angles (Fig. 3, left panel). As a first step we used the NACO astrometry to determine the central position of the primary, being itself outside the observed field of view of the integral field observations. The orientation of the SINFONI observations was intentionally chosen to leave the connection line of primary and companion exactly in x direction, the primary is about 1.85 arcsec exactly to the left of CVSO 30 c in the data, because the x direction offers a twice as good sampling regarding the number of pixels for the separation. We were thus able to subtract the radial symmetric halo of the host star from the data cube (Fig. 3, central panel), using the nominal spatial scale. This is necessary as the halo of

Table 6. Photometric rejection significance, spectroscopic reduced χ^2 results and corresponding formal significance without systematics for different comparison objects

Object	SpT	Photometry		add. ref.	Spectroscopy	
		J-H [σ]	H-Ks [σ]		H-band [σ/χ^2]	K-band [σ/χ^2]
HD 237903	K7V	3.4	0.5	[1]	>6/2.66	>6/1.60
Gl 846	M0V	2.8	1.8	[1]	>6/2.38	5.4/1.51
Gl 229	M1V	0.6	0.3	[1]	>6/2.37	5.3/1.50
Gl 806	M2V	4.5	2.5	[1]	>6/2.73	4.3/1.40
Gl 388	M3V	3.7	2.8	[2],[1]	>6/2.57	3.7/1.33
Gl 213	M4V	5.5	2.6	[2],[1]	>6/2.80	2.5/1.21
Gl 51	M5V	3.8	3.5	[2],[1]	>6/2.47	2.6/1.21
Gl 406	M6V	3.4	4.6	[2],[1]	>6/2.50	2.5/1.20
Gl 644C	M7V	4.1	5.1	[2],[1]	>6/2.87	2.2/1.17
Gl 752B	M8V	2.6	6.4	[2],[1]	>6/2.76	2.3/1.18
LHS 2065	M9V	1.7	7.5	[1]	>6/2.45	2.2/1.17
LHS 2924	L0	1.4	6.5	[2],[1]	>6/2.77	2.1/1.16
2MUCD 20581	L1	2.2	7.5	[2]	>6/3.96	3.7/1.33
Kelu-1AB	L2+L3.5	2.2	9.8	[2]	>6/3.68	3.6/1.32
2MUCD 11291	L3	1.8	>10	[2]	>6/3.66	3.8/1.34
2MUCD 12128	L4.5	5.5	>12	[2]	>6/3.09	3.4/1.29
2MUCD 11296	L5.5	1.3	>10	[2]	>6/4.60	5.5/1.52
2MUCD 11314	L6	2.0	8.4	[2]	>6/3.64	>6/1.66
2MUCD 10721	L7.5	5.8	>11	[2]	>6/3.49	3.4/1.29
2MUCD 10158	L8.5	2.5	9.8	[2]	>6/4.87	5.0/1.47
SDSS 1520+354	T0	1.0	5.4	[3]	>6/4.63	>6/2.15
SDSS 0909+652	T1.5	0.3	0.4	[4]	>6/8.04	>6/3.64
SDSS 1254-012	T2	0.8	2.0	[2]	>6/7.97	>6/2.90
2MASS 055-140	T4	9.4	0.1	[2]	>6/16.2	>6/19.1
HD 204585	M4.5III	0.4	0.8	[1]	>6/1.86	>6/1.88
HD 175865	M5III	0.1	0.5	[1]	>6/1.91	>6/1.78
Galaxies	various	4.2	3.0	[5],[6]	>6/2.28	>6/1.61
Quasars	—	4.4	3.9	[5]	—	—
White Dwarfs	various	6.4	3.9	[5]	—	—
CVSO 30	M3	2.7	1.7	—	>6/3.31	6.0/1.57
PZ Tel B	M7	2.1	1.4	[7]	>6/3.29	3.0/1.25
CT Cha b	M9	0.4	1.3	[8],[9]	>6/2.27	1.8/1.13
2M0441 Bb	L1	0.5	2.4	[10]	>6/3.13	1.9/1.13
1RXS 1609 b	L4	1.1	3.0	[11]	>6/2.70	2.3/1.18
β Pic b	L4	1.0	3.5	[12]	>6/2.06	—
2M1207 b	L7	3.5	4.4	[13]	>6/2.66	2.5/1.20
S Ori 64	L/T	0.9	0.7	[14]	—	—
DP (Fig. 4)	—	—	—	[15]	2.2/1.16	2.0/1.14

References: [1] Rayner et al. (2009), [2] Cushing et al. (2005), [3] Burgasser et al. (2010a), [4] Chiu et al. (2006), [5] Hewett et al. (2006), [6] Mannucci et al. (2001), [7] Schmidt et al. (2014), [8] Schmidt et al. (2009), [9] Schmidt et al. (2008), [10] Bowler & Hillenbrand (2015), [11] Lafrenière et al. (2008), [12] Chilcote et al. (2015), [13] Patience et al. (2010), [14] Peña Ramírez et al. (2012), from VISTA to 2MASS magnitudes using colour equations from <http://casu.ast.cam.ac.uk/surveys-projects/vista/technical/photometric-properties>, [15] Helling et al. (2008).

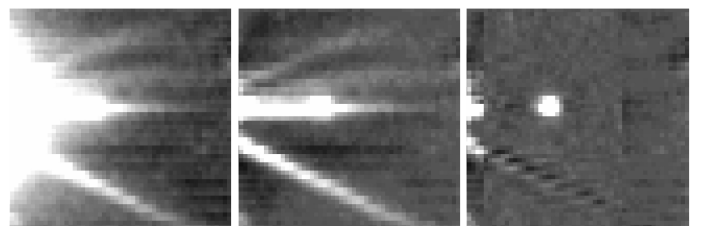


Fig. 3. Median in wavelength direction of the reduced VLT/SINFONI integral field cubes. *Left:* Cube after reduction. *Center:* Cube after removal of the primary halo, assumed to be centered at the separation of 1.85'', as measured in the VLT/NACO images. North is about 70° from the right hand side towards the bottom of the plots. *Right:* Cube after removal of primary halo, spectral deconvolution and polynomial flattening of the resultant background, used for the extraction of the final spectrum.

the primary star is determined by the AO performance at the different wavelength. At this stage we extracted a first spectrum by subtracting an average spectrum of the spike, left and right of the companions psf from the superposition of companion and spike. We find the results in Fig. A.2 before (red spectrum) and after

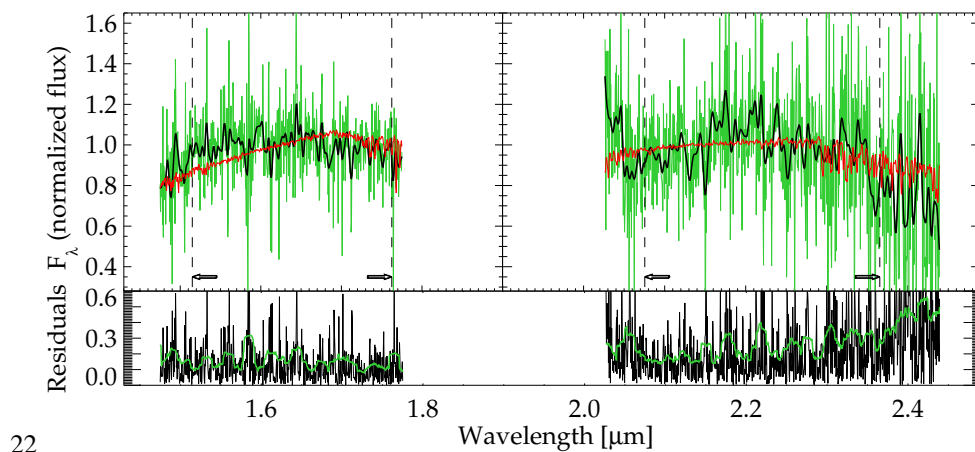


Fig. 4. Spectrum of CVSO 30 c, as extracted from the spectral deconvolution corrected cube in the right panel of Fig. 3. *Top:* The spectrum in resolution 700 (black) is shown after binning of the original extracted spectrum in resolution 1500 (green). The best-fitting Drift-Phoenix model Helling et al. (2008) is shown in red, fitting both the individually normalized H and K spectra. This type of normalization was necessary as the redder color of the models, in comparison to the unusually blue nature of CVSO 30 c, would steer the best-fitting model to higher temperatures, unable to fit the individual features present in H and K band. The best-fitting model (red) corresponds to 1600 K, surface gravity $\log g$ 3.6 dex, metallicity $[M/H]$ 0.3 dex and 0.19 mag of visual extinction. *Bottom:* Absolute value of the difference between spectrum and model from the top panel (black) versus noise floor at the corresponding position (green).

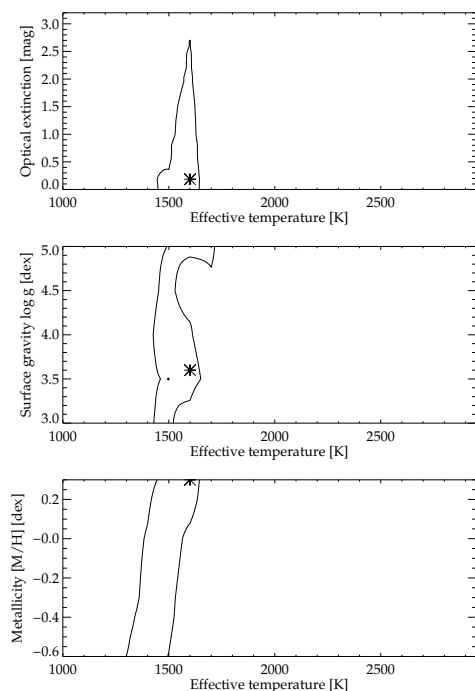


Fig. 5. 1σ contour plots of the χ^2 Drift-Phoenix model fit to the spectrum shown in Fig. 4. Contour plot in extinction vs. effective temperature (top), surface gravity $\log g$ vs. effective temperature (center) and metallicity $[M/H]$ vs. effective temperature (bottom). The fit shows a best fit at 1600 K, low extinction of 0.19 mag, higher values getting less and less likely and a best fit at $\log g$ 3.6. While all surface gravities seem to be almost of equal probability, a high surface gravity foreground brown dwarf can be excluded from the shape of the H-band in Fig. 6. Although the young planetary models differ in photometric colors, this could be because of a not yet fully understood change in the cloud properties at the L-T transition, indicated by the change in brightness of the L-T transition with age of the system, shown in Fig. 11.

(blue spectrum) spike subtraction, which also removes the still present OH lines. The horizontal spike in Fig. 3 appears to narrow to the right. This is a projection effect as the rotation of the

spike within the 3 median combined cubes leads to less overlap on the right hand side of the cube than on the left hand side. For this reason the continuum in Fig. A.2 is not trustworthy, as the flux of the spike below the companion candidate is not the average of the spike flux left and right of the object.

We tried several methods to remove the spike and decided to follow the spectral deconvolution technique (Sparks & Ford 2002; Thatte et al. 2007), a method able to discriminate both the wavelength dependent airy rings and speckles, as well as the spike from the light of the wavelength-independent companion position by using the long wavelength coverage of the observed data cube. As given in Thatte et al. (2007) for the same instrument the bifurcation radius for SINFONI H+K is for $\epsilon=1.1$ $r=246$ mas, and for $\epsilon=1.2$ $r=268$ mas, so parts of the data without contamination of the companion could be found at the much higher separation of about 1.85 arcsec. The reduction was then completed by applying a polynomial background correction around CVSO 30 c, as the previous reduction steps left a low-spatial frequency remnant around it (Fig. 3, right panel), and finally the optimal extraction algorithm (Horne 1986) performed around the companion and subtracted by the corresponding background flux from the close, well corrected vicinity, and the telluric atmosphere correction using HD 61957, a B3V spectroscopic standard observed in the same night.

We first compare the spectrum of CVSO 30 c to spectra derived from Drift-Phoenix atmosphere simulations, dedicated radiative transfer models that take into account the strong continuum altering influence of dust cloud formation in the detectable parts of planetary atmospheres (Helling et al. 2008). From a χ^2 comparison of the H- and K-band spectra to the model grid, we find an effective temperature of about 1800 - 1900 K, while the individual fit of the H-band spectrum as well as the K-band spectrum give a lower T_{eff} of about 1600 K. In addition, the slope of the blue part of the triangular H-band is too steep in the atmosphere models of about 1800 K and does not fit the continuum well. The higher T_{eff} is only needed to fit the unusually blue H-Ks color of the object, as already discussed in the previous photometry section and visible in Fig. 2, since the models do not include a good description of the dust opacity drop at the L-T transition, yet. We thus decided to fit the H- and K-band simul-

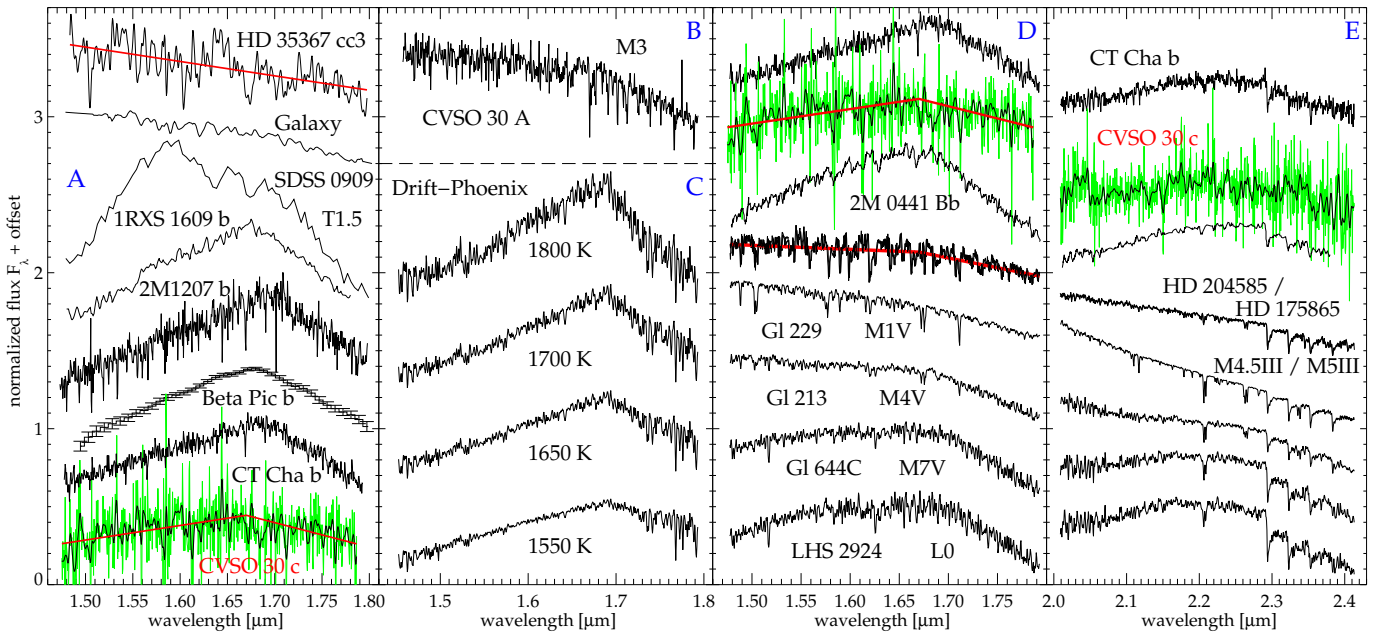


Fig. 6. H-band spectrum of CVSO 30 c (lower left) compared to several known planetary candidates and background objects (subplots A, D, E). The triangular shape of the H-band (A), with red linear fits guiding the eye, indicates that it is not a background galaxy, but a sub-stellar companion. Beta Pic b has approximately the same luminosity and temperature (Chilcote et al. 2015), however a different surface gravity, hence about twice the mass of CVSO 30 c. As shown (C) the Drift-Phoenix models indicate that the H-band becomes less steep with temperature. This means CVSO 30 c is even slightly lower in temperature than β Pic b. In the upper left another candidate is shown, detected at $4.3''$ from the A1 star HD 35367, being about 0.5 mag brighter in the K-band than CVSO 30 c, but obviously in the background. In addition the H-band (D) and K-band (E) of CT Cha b and 2M 0441 Bb, the best-fitting comparison objects in K-band are given. Both and CVSO 30 c in (D, E) with identical offsets in H-band and K-band. Additionally the best-fitting giants and a sample of late type dwarfs is shown for comparison. References and individual reduced χ_r^2 comparison values are given in Table 6. Low-res spectra of free-floating planetary candidates are not shown, but can be found in Martín et al. (2001).

taneously, but normalizing them individually, to cope with the unusual colors, while using all the present information for the fit. In this way we find a best fitting $T_{\text{eff}} = 1600^{+120}_{-300}$ K, an extinction $A_V = 0.19^{+2.51}_{-0.19}$ mag, a surface gravity $\log g [\text{cm/s}^2] = 3.6^{+1.4}_{-0.6}$ dex and a metallicity $\log[(M/H)/(M/H)_\odot] = 0.3_{-0.9}$ dex at the upper supersolar edge of the grid. The 1σ fitting contours can be found in Fig. 5, showing the full regime for the error bars, and the best fit itself is shown in Fig. 4.

In Fig. 6 we compare the spectrum of CVSO 30 c to the triangular shaped H-band spectrum of the β Pic b planet, obtained with the Gemini Planet Imager (GPI, Chilcote et al. 2015), as well as to other planetary mass objects. β Pic b is particularly suited as comparison object, as it is young (10–20 Myr), and has about the same luminosity and effective temperature (1600–1700 K), while being of higher mass (10–12 M_{Jup}). We show linear fits to the blue and red part of the H-band as well as the triangular shape of chosen Drift-Phoenix models. In contrast to M5 – L5 companions, for which the H_2O index in Allers et al. (2007) shows an increase in water absorption, the absorption gets shallower for later spectral types. This means that even though the formal χ^2 fit finds a best temperature of 1600 K for CVSO 30 c, the temperature is likely to be lower than for β Pic b, exhibiting a steeper H-band spectrum. The object’s spectrum is not consistent with a giant of any spectral type. The best fitting giants with consistent photometry (Fig. 2 & Table 6) are shown as comparison in Fig. 6 and would be at a distance of about 200 Mpc. To improve the fit in the K band the spectral type would have to be later than M7III, while the H band does not fit for these objects. Finally CVSO 30 c, being comparable but younger, must have a lower surface gravity than β Pic b, determined to have a 1σ upper

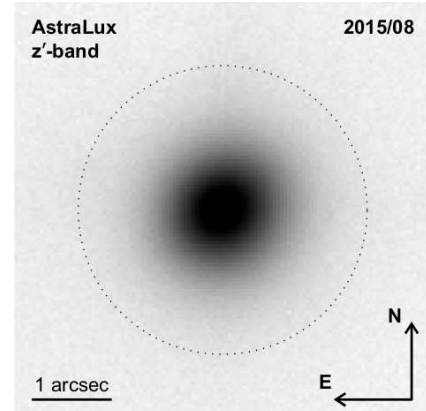


Fig. 7. AstraLux z' band image of CVSO 30, taken on Aug 27th 2015. The dotted circle indicates an angular separation of 1.8 arcsec to CVSO 30 (see Fig. 8). Beside the star, which is located in the center of the AstraLux image, no further objects are detected.

limit of $\log g [\text{cm/s}^2] = 4.3$ dex according to the linear prior orbit fit in Bonnefoy et al. (2014b). This corrects the surface gravity of CVSO 30 c to $\log g [\text{cm/s}^2] = 3.6^{+0.7}_{-0.6}$ dex.

5. AstraLux lucky imaging follow-up observations

We performed follow-up of CVSO 30 with 2000 s of AstraLux integration in z' . The individual AstraLux images were combined using our own pipeline for the reduction of lucky imaging data. The fully reduced AstraLux image is shown in Fig. 7. z'

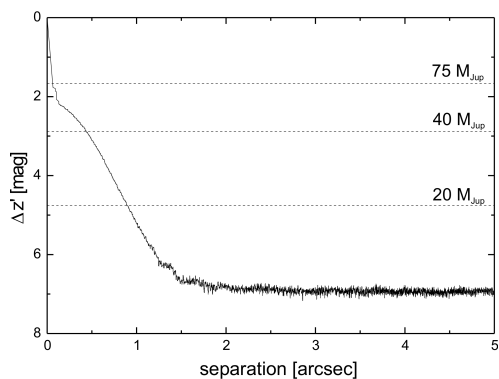


Fig. 8. The $S/N=5$ detection limit of our AstraLux observation of CVSO 30 (Fig. 7). The reached magnitude difference dependent on the angular separation to the star is shown. The horizontal dashed lines indicate the expected magnitude differences of sub-stellar companions of the star at an age of 3 Myr. Beyond about 1.8 arcsec (or ~ 640 au of projected separation) all companions with masses down to $10 M_{\text{Jup}}$ can be excluded around CVSO 30.

photometry of CVSO 30 was not measured so far, but can be derived from its magnitudes in other photometric bands using the color transformation equations¹ from Jordi et al. (2006). The V and R band photometry of CVSO 30, as given by Briceño et al. (2005) and van Eyken et al. (2012) ($V = 16.26 \pm 0.19$ mag, and $R = 15.19 \pm 0.085$ mag), and the I band photometry of the star, listed in the 2005 DENIS database ($I = 13.695 \pm 0.030$ mag), yield $z' = 13.66$ mag.

The ($S/N=5$) detection limit reached in the AstraLux observation is given in Fig. 8. At an angular separation of about 1.8 arcsec from CVSO 30 (or ~ 640 au of projected separation) companions, which are $\Delta z' = 6.8$ mag fainter than the star, are still detectable at $S/N=5$. The reached detection limit at this angular separation is $z' = 20.5$ mag, which is just a tenth of magnitude above the limiting magnitude in the background noise limited region around the star at angular separations larger than 2 arcsec. This results in a limiting absolute magnitude of $M_{z'} = 12.7$ mag, allowing the detection of sub-stellar companions of the star with masses down to $10 M_{\text{Jup}}$ according to Baraffe et al. (2015) evolutionary models.

Further the AstraLux observations also exclude all young (3 Myr) stellar objects (mass larger than $75 M_{\text{Jup}}$) unrelated to CVSO 30, which are located in the AstraLux field of view at distances closer than about 3410 pc. All young M dwarfs with an age of 3 Myr and masses above $15 M_{\text{Jup}}$ ($T_{\text{eff}} > 2400$ K) can be ruled out up to 530 pc, respectively. All old stellar objects (mass larger than $75 M_{\text{Jup}}$) with an age of 5 Gyr can be excluded, which are located closer than about 130 pc.

The AstraLux upper limit results in $z' - K_s \geq 1.75$ mag, which corresponds to exclusion of $\geq 0.2 M_{\odot}$ or ≥ 3300 K (Baraffe et al. 2015) as possible source or about earlier than M4.5V in spectral type (Kenyon & Hartmann 1995). As any object later than $\sim M2V/M3V$ can be excluded by $\geq 4\sigma$ from JHKs photometry (Table 6), no type of M dwarf can be a false positive of the new companion candidate CVSO 30 c.

6. Mass determination and conclusions

With the object brightness determined from the direct near-IR imaging and the information provided by the spectroscopic analysis, we can directly estimate the basic parameters of CVSO 30

c. To determine the luminosity we considered the extinction law by Rieke & Lebofsky (1985), a bolometric correction of $B.C._K = 3.3^{+0.0}_{-0.7}$ mag for spectral type L5-T4 (Golimowski et al. 2004), and a distance of 357 ± 52 pc to the 25 Orion cluster. From the 2MASS brightness of the primary and the differential brightness measured in our VLT NACO data (Table 2) as well as the extinction value towards the companion derived from spectroscopy, we find $\log L_{\text{bol}}/L_{\odot} = -3.78^{+0.33}_{-0.13}$ dex. From the luminosity and effective temperature, we calculate the radius to be $R = 1.63^{+0.87}_{-0.34} R_{\text{Jup}}$. In combination with the derived surface gravity this would correspond to a mass of $M = 4.3 M_{\text{Jup}}$, dominated in its errors by high distance and surface gravity uncertainties. While the latter value and the photometry (Fig. 2) would be consistent with a high surface gravity, thus old foreground T-type brown dwarf, but inconsistent with an L-type brown dwarf, the available spectroscopy excludes an old T-type brown dwarf (Fig. 6 & Table 6). While the photometry is also consistent with early M dwarfs, the K-band spectroscopy and z' upper limit show the opposite behaviour, being only consistent with late M dwarfs, excluding all types with high significance. Similarly the remaining H-band spectroscopy excludes all comparison objects. Only the best-fitting Drift-Phoenix model (Fig. 4) shows low deviation in H-band, consistent with the fact that the only available very young directly imaged planet candidates exhibit higher temperatures, thus a steeper H-band (Fig. 6).

Although recent observations by Yu et al. (2015) cast doubt on the existence of the inner transiting planet candidate CVSO 30 b or PTF0 8-8695 b, we assume its existence throughout the remaining discussion, as there are difficulties for all 5 hypotheses to reproduce the observations presented in Yu et al. (2015), including e.g. different types of starspots. The inner planet hypothesis gives another constraint, namely that the system has to be stable with both its planets. As described in van Eyken et al. (2012), CVSO 30 b is very close to its Roche radius, the radius of stability. Assuming the values for mass of CVSO 30 b, its radius and orbital period (Tables 2 & 3), we find from the Roche limit an upper limit for the mass of CVSO 30 of $\leq 0.92 M_{\odot}$ for a stable inner system comprised of CVSO 30 A & b. This mass limit for CVSO 30 is fulfilled at 1 Myr for masses of CVSO 30 c of $\leq 6.9 M_{\text{Jup}}$ at ≤ 760 pc up to 5.8 Myr with masses of CVSO 30 c of $\leq 9.2 M_{\text{Jup}}$ at ≤ 455 pc, according to BT-Settl evolutionary models (Allard 2014; Baraffe et al. 2015). Higher ages are not consistent with the age estimate of the primary, however even at 20 Myr we find a mass of CVSO 30 c of $\leq 12.1 M_{\text{Jup}}$ at ≤ 340 pc. With the Roche stability criterion for CVSO 30 b the previous calculations result in a mass estimate of $M = 4.3^{+4.9}_{-3.7} M_{\text{Jup}}$ for CVSO 30 c.

For the approximate age of CVSO 30 2–3 Myr BT-Settl evolutionary models (Allard 2014; Baraffe et al. 2015) predict an apparent brightness of $m_K \sim 18.5$ mag (assuming the distance to 25 Ori), effective temperature ~ 1575 K, mass 4–5 M_{Jup} and $\log L_{\text{bol}}/L_{\odot} \sim -3.8$ dex. These expected values are very close to the best fit atmospheric model spectra fits above and even the derived visual extinction of about 0.19 mag is very close to the value of the primary ~ 0.12 mag (Briceño et al. 2005).

Of course, these evolutionary models can also be used to determine the resulting mass from the luminosity and age of the companion candidate and system, respectively. To put CVSO 30 c into context we show the models and several of the currently known directly imaged planet candidates in Fig. 9. The new companion is one of the youngest and lowest mass companions and we find a mass of $4.7^{+5.5}_{-2.0} M_{\text{Jup}}$, as the luminosity is not very precise, because of the rather scarce knowledge of the distance of the system. However, if we take additionally temper-

¹ $r - R = 0.77 \cdot (V - R) - 0.37$ and $r - z' = 1.584 \cdot (R - I) - 0.386$

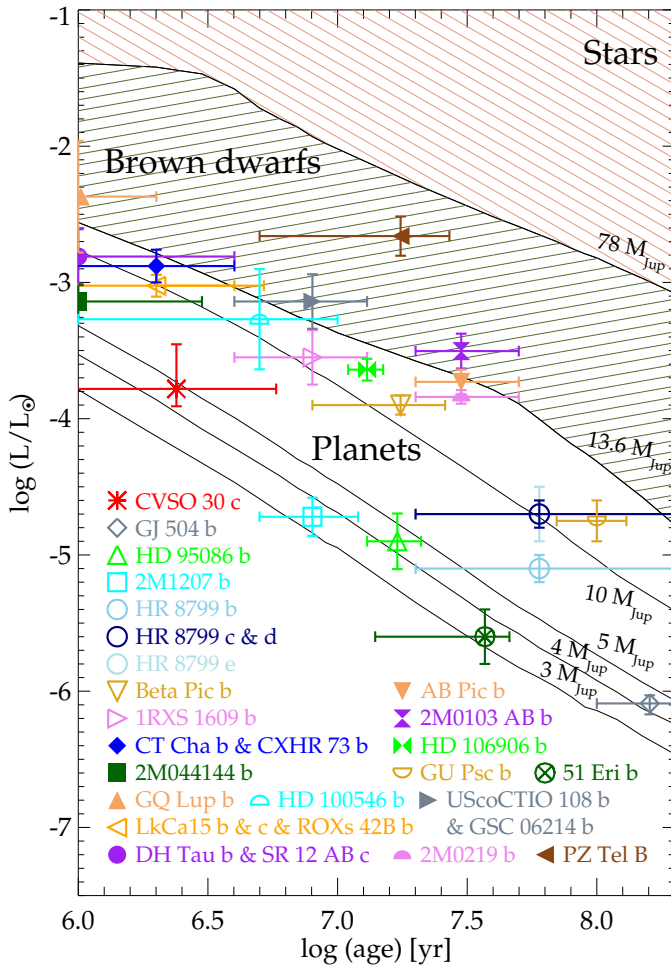


Fig. 9. Evolution of young stars, brown dwarf and planets with BT-Settl evolutionary tracks (Allard 2014; Baraffe et al. 2015). Shown are a few of the so far known planet candidates in comparison to the new substellar companion candidate CVSO 30 c (see Table A.1).

ature into account, we find a more precise mass determination of $4.7^{+3.6}_{-2.0} M_{\text{Jup}}$, putting CVSO 30 c well into the planetary regime and being very close in mass to the probable inner companion of the system CVSO 30 b with about $2.8 - 6.9 M_{\text{Jup}}$ (van Eyken et al. 2012; Barnes et al. 2013).

In Fig. 10 we show the reached depth per pixel in the Ks band epoch of 20.2 mag, corresponding to $2.8 M_{\text{Jup}}$ at the age of CVSO 30, using the same models as above. Brown dwarfs could be found from 30 au outwards, planets from 79 au outwards and CVSO 30 c could have been found from 171 au outwards.

The core accretion model (Safronov & Zvjagina 1969; Goldreich & Ward 1973; Pollack et al. 1996), one of the much debated planet formation scenarios, is unlikely to form an object in situ at ≥ 660 au, as the time-scale would be prohibitively long at such separations. In principle the object could have also formed in a star-like fashion by turbulent core fragmentation as in the case of a binary star system, since the opacity limit for fragmentation is a few Jupiter masses (Bate 2009), however, the large separation and high mass ratio argue against this hypothesis.

The even more obvious possibility would be planet-planet scattering as an inner planet candidate CVSO 30 b of comparable mass is present, that could have been scattered inward at the very same scattering event. Several authors simulated such events and found mostly high eccentric orbits for the outer scattered planets

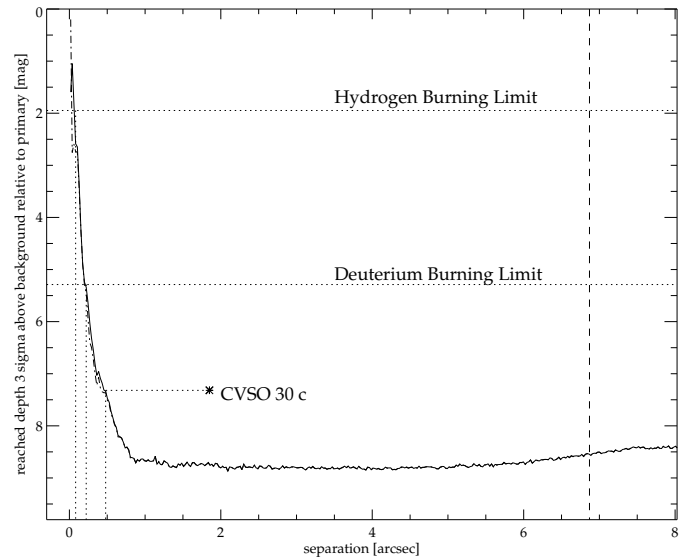


Fig. 10. Dynamic range per pixel achieved in our VLT/NACO Ks band observations, given as 3σ contrast to the primary star. The companion would have been detectable till 0.48 arc seconds or 171 au separation. A depth of 20.2 mag was reached at maximum, corresponding to $2.8 M_{\text{Jup}}$.

up to 100s or 1000s of au (Stamatellos & Whitworth 2009; Nagasawa & Ida 2011), comparable to our outer planet candidate minimum separation of 660 au. The closest match to CVSO 30 bc of a model simulation was presented by Nagasawa & Ida (2011) with an object at ~ 300 au, having an inner hot planet with which it was scattered. Scattering or gravitational interaction might not be that uncommon as $72\% \pm 16\%$ of hot Jupiters are part of multi-planet and/or multi-star systems (Ngo et al. 2015).

The luminosity of CVSO 30 c is only consistent with “hot-start” models, usually representing the objects formed by gravitational disk-instability, not with cold-start models attributed to core accretion formed planets (Marley et al. 2007). However, as stated in Spiegel & Burrows (2012) first-principle calculations cannot yet specify with certainty what the initial (post-formation) entropies of objects should be in the different formation scenarios, hence CVSO 30 c could have formed via gravitational disk-instability or core accretion and be scattered with CVSO 30 b afterwards.

In this context it would also be important to clarify the nature of the unusually blue H-Ks color of CVSO 30 c. It is consistent with colors of free-floating planets (Fig. 2) and could be caused by its youth, allowing the companion to be very bright, still already being at the L-T transition, consistent with simulations of cluster brown dwarfs at very young ages and their colors in Saumon & Marley (2008) (Fig. 11). This would imply a temperature at the lower end of the 1σ errors found for CVSO 30 c, ≤ 1400 K, which is however consistent with the less steep H-band in comparison to β Pic b of about 1600–1700K (Chilcote et al. 2015), as shown in Fig. 6. For old brown dwarfs the L-T transition occurs at $T_{\text{eff}} 1200\text{--}1400$ K, when methane absorption bands start to be ubiquitously seen. However, in the ~ 30 Myr old planet candidates around HR 8799 no strong methane is found, while the spectrum of the ~ 90 Myr old object around GU Psc shows strong methane absorption (Naud et al. 2014), all at temperatures of about 1000–1100 K. Thus the L-T transition might be gravity dependent (Marley et al. 2012). Binarity of

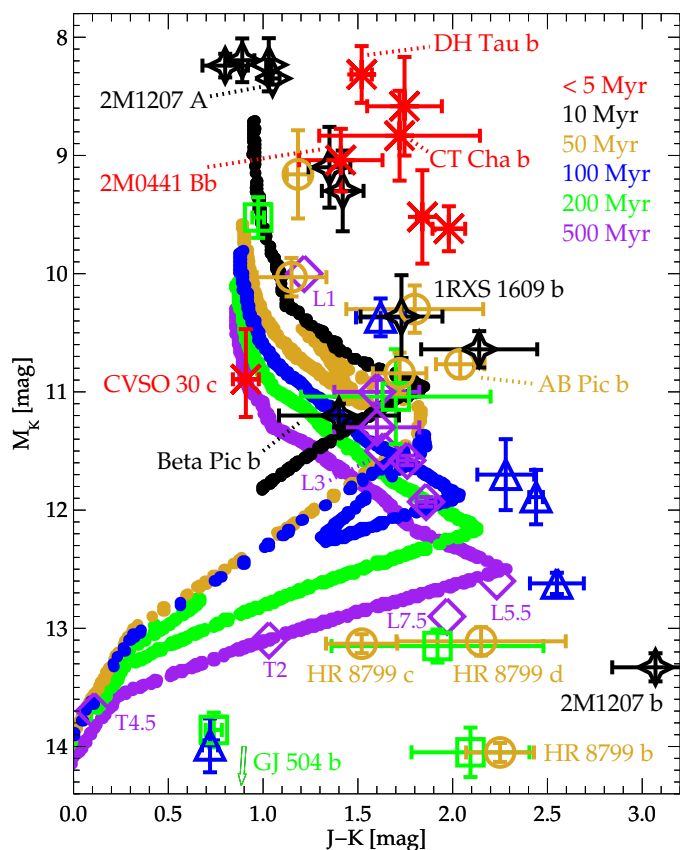


Fig. 11. Color-magnitude diagram of simulated cluster brown dwarf population from Saumon & Marley (2008). Each sequence corresponds to a different age as given in the legend. Superimposed the position several planet candidates and CVSO 30 c. Its unusual blue color can most likely be attributed to its youth, being about 2.4 Myr. The younger the objects, the brighter they are because of not yet occurred contraction. Hence they reach the L- and T-dwarf regime at higher brightnesses. If this extrapolation is correct CVSO 30 c is already at the L-T transition, roughly consistent with its low effective temperature results. See discussion, Table A.2 & Fig. A.5 for details.

CVSO 30 c can also not be excluded yet, which would explain the unusual blue H-Ks color, too.

Since there is no way to confirm that CVSO 30 c is co-moving with its host star from our proper motion analysis we cannot exclude the possibility that CVSO 30 c is a free-floating young planet belonging to the 25 Ori cluster, which is not gravitationally bound to CVSO 30. However, such a coincidence is rather improbable. In Zapatero Osorio et al. (2000) 847 arcmin² of the σ Orionis star cluster were searched for free-floating planets and only 6 candidates were found in the survey having comparable colors as CVSO 30 c has. Thus the probability to find by chance a free-floating planet within a radius of 1.85'' around the transiting planet host star CVSO 30 is about $2 \cdot 10^{-5}$.

With a mass ratio of planet candidate to star $q = 0.0115 \pm 0.0015$ CVSO 30 c (and CVSO 30 b) is among the lowest mass ratio imaged planets (see e.g. De Rosa et al. 2014).

In summary, CVSO 30 b and c allow for the first time a comprehensive study of both a transiting and a directly imaged planet candidate within the same system, hence at the same age and even comparable masses, using RV, transit photometry, direct imaging and spectroscopy. Within a few years the GAIA satellite mission (Perryman 2005) will provide the distance to the system to a precision of about 10 pc, further restricting the

mass of CVSO 30 c. Simulations of a possible scattering event will profit from the current (end) conditions found for the system. Considering that the inner planet is very close to the Roche stability limit and the outer one is far away from its host star, the future evolution and stability of the system is also very interesting for dedicated modelling. To investigate how often such scattering events occur, a search for inner planets also around other stars with directly imaged wide planets should be conducted.

Acknowledgements. We thank the ESO and CAHA staff for support, especially during service mode observations. Moreover, we would like to thank Jeff Chilcote & David Lafrenière for kindly providing electronic versions of comparison spectra from their publications and the anonymous referee as well as editor T. Forveille for helpful comments to improve this manuscript. TOBS and JHMMS acknowledge support by the DFG Graduiertenkolleg 1351 “Extrasolar Planets and their Host Stars”. RN and SR would like to thank DFG for support in the Priority Programme SPP 1385 on the “First Ten Million Years of the Solar system” in project NE 515/33-1. SR is currently a Research Fellow at ESA/ESTEC. This publication makes use of data products from the Two Micron All Sky Survey, which is a joint project of the University of Massachusetts and the Infrared Processing and Analysis Center/California Institute of Technology, funded by the National Aeronautics and Space Administration and the National Science Foundation. This research has made use of the VizieR catalog access tool and the Simbad database, both operated at the Observatoire Strasbourg. This research has made use of NASA’s Astrophysics Data System.

List of Objects

‘CVSO 30’ on page 2

References

- Adams, F. C. & Laughlin, G. 2001, *Icarus*, 150, 151
- Allard, F. 2014, in *IAU Symposium*, Vol. 299, IAU Symposium, ed. M. Booth, B. C. Matthews, & J. R. Graham, 271–272
- Aller, K. M., Kraus, A. L., Liu, M. C., et al. 2013, *ApJ*, 773, 63
- Allers, K. N., Jaffe, D. T., Luhman, K. L., et al. 2007, *ApJ*, 657, 511
- Andrews, S. M., Rosenfeld, K. A., Kraus, A. L., & Wilner, D. J. 2013, *ApJ*, 771, 129
- Artigau, É., Gagné, J., Faherty, J., et al. 2015, *ApJ*, 806, 254
- Baglin, A., Auvergne, M., Barge, P., et al. 2007, in *American Institute of Physics Conference Series*, Vol. 895, Fifty Years of Romanian Astrophysics, ed. C. Dumitrache, N. A. Popescu, M. D. Suran, & V. Mior, 201–209
- Bailey, V., Meshkat, T., Reiter, M., et al. 2014, *ApJ*, 780, L4
- Baraffe, I., Homeier, D., Allard, F., & Chabrier, G. 2015, *A&A*, 577, A42
- Barnes, J. W., van Eyken, J. C., Jackson, B. K., Ciardi, D. R., & Fortney, J. J. 2013, *ApJ*, 774, 53
- Bate, M. R. 2009, *MNRAS*, 392, 590
- Béjar, V. J. S., Zapatero Osorio, M. R., Pérez-Garrido, A., et al. 2008, *ApJ*, 673, L185
- Billler, B. A., Liu, M. C., Wahhaj, Z., et al. 2010, *ApJ*, 720, L82
- Binks, A. S. & Jeffries, R. D. 2014, *MNRAS*, 438, L11
- Bonavita, M., Daemgen, S., Desidera, S., et al. 2014, *ApJ*, 791, L40
- Bonnefoy, M., Boccaletti, A., Lagrange, A.-M., et al. 2013, *A&A*, 555, A107
- Bonnefoy, M., Chauvin, G., Lagrange, A.-M., et al. 2014a, *A&A*, 562, A127
- Bonnefoy, M., Marleau, G.-D., Galicher, R., et al. 2014b, *A&A*, 567, L9
- Borucki, W. J., Koch, D., Basri, G., et al. 2010, *Science*, 327, 977
- Boss, A. P. 1997, *Science*, 276, 1836
- Boss, A. P. 2006, *ApJ*, 637, L137
- Bowler, B. P. & Hillenbrand, L. A. 2015, *ApJ*, 811, L30
- Bowler, B. P., Liu, M. C., Shkolnik, E. L., & Dupuy, T. J. 2013, *ApJ*, 774, 55
- Bowler, B. P., Liu, M. C., Shkolnik, E. L., & Tamura, M. 2015, *ApJS*, 216, 7
- Briceño, C., Calvet, N., Hernández, J., et al. 2005, *AJ*, 129, 907
- Briceño, C., Hartmann, L., Hernández, J., et al. 2007a, *ApJ*, 661, 1119
- Briceño, C., Preibisch, T., Sherry, W. H., et al. 2007b, *Protostars and Planets V*, 345
- Broeg, C., Schmidt, T. O. B., Guenther, E., et al. 2007, *A&A*, 468, 1039
- Burgasser, A. J., Cruz, K. L., Cushing, M., et al. 2010a, *ApJ*, 710, 1142
- Burgasser, A. J., Simcoe, R. A., Bochanski, J. J., et al. 2010b, *ApJ*, 725, 1405
- Burningham, B., Leggett, S. K., Homeier, D., et al. 2011, *MNRAS*, 414, 3590
- Cameron, A. G. W. 1978, *Moon and Planets*, 18, 5
- Carson, J., Thalmann, C., Janson, M., et al. 2013, *ApJ*, 763, L32
- Charbonneau, D., Brown, T. M., Latham, D. W., & Mayor, M. 2000, *ApJ*, 529, L45
- Chauvin, G., Lagrange, A.-M., Dumas, C., et al. 2004, *A&A*, 425, L29

- Chauvin, G., Lagrange, A.-M., Dumas, C., et al. 2005a, *A&A*, 438, L25
- Chauvin, G., Lagrange, A.-M., Lacombe, F., et al. 2005b, *A&A*, 430, 1027
- Chauvin, G., Lagrange, A.-M., Zuckerman, B., et al. 2005c, *A&A*, 438, L29
- Chilcote, J., Barman, T., Fitzgerald, M. P., et al. 2015, *ApJ*, 798, L3
- Chiu, K., Fan, X., Leggett, S. K., et al. 2006, *AJ*, 131, 2722
- Close, L. 2010, *Nature*, 468, 1048
- Close, L. M., Siegler, N., Freed, M., & Biller, B. 2003, *ApJ*, 587, 407
- Close, L. M., Zuckerman, B., Song, I., et al. 2007, *ApJ*, 660, 1492
- Currie, T., Burrows, A., & Daemgen, S. 2014, *ApJ*, 787, 104
- Cushing, M. C., Rayner, J. T., & Vacca, W. D. 2005, *ApJ*, 623, 1115
- Cutri, R. M., Skrutskie, M. F., van Dyk, S., et al. 2003, 2MASS All Sky Catalog of point sources.
- De Rosa, R. J., Patience, J., Ward-Duong, K., et al. 2014, *MNRAS*, 445, 3694
- Delorme, P., Gagné, J., Girard, J. H., et al. 2013, *A&A*, 553, L5
- Diolaiti, E., Bendinelli, O., Bonaccini, D., et al. 2000, in *Society of Photo-Optical Instrumentation Engineers (SPIE) Conference Series*, Vol. 4007, Society of Photo-Optical Instrumentation Engineers (SPIE) Conference Series, ed. P. L. Wizinowich, 879–888
- Downes, J. J., Briceño, C., Matese, C., et al. 2014, *MNRAS*, 444, 1793
- Ducourant, C., Teixeira, R., Chauvin, G., et al. 2008, *A&A*, 477, L1
- Dupuy, T. J., Liu, M. C., & Ireland, M. J. 2014, *ApJ*, 790, 137
- Errmann, R., Raetz, S., Kitz, M., Neuhäuser, R., & YETI Team. 2014, *Contributions of the Astronomical Observatory Skalnaté Pleso*, 43, 513
- Faherty, J. K., Rice, E. L., Cruz, K. L., Mamajek, E. E., & Núñez, A. 2013, *AJ*, 145, 2
- Ford, E. B. & Rasio, F. A. 2008, *ApJ*, 686, 621
- Freistetter, F., Krivov, A. V., & Löhne, T. 2007, *A&A*, 466, 389
- Galicher, R., Rameau, J., Bonnefoy, M., et al. 2014, *A&A*, 565, L4
- Gauza, B., Béjar, V. J. S., Pérez-Garrido, A., et al. 2015, *ApJ*, 804, 96
- Gizis, J. E., Allers, K. N., Liu, M. C., et al. 2015, *ApJ*, 799, 203
- Goldreich, P. & Ward, W. R. 1973, *ApJ*, 183, 1051
- Golimowski, D. A., Leggett, S. K., Marley, M. S., et al. 2004, *AJ*, 127, 3516
- Helling, C., Dehn, M., Woitke, P., & Hauschildt, P. H. 2008, *ApJ*, 675, L105
- Hernández, J., Briceño, C., Calvet, N., et al. 2006, *ApJ*, 652, 472
- Hernández, J., Calvet, N., Hartmann, L., et al. 2005, *AJ*, 129, 856
- Hewett, P. C., Warren, S. J., Leggett, S. K., & Hodgkin, S. T. 2006, *MNRAS*, 367, 454
- Hinkley, S., Pueyo, L., Faherty, J. K., et al. 2013, *ApJ*, 779, 153
- Horne, K. 1986, *PASP*, 98, 609
- Ireland, M. J., Kraus, A., Martinache, F., Law, N., & Hillenbrand, L. A. 2011, *ApJ*, 726, 113
- Itoh, Y., Hayashi, M., Tamura, M., et al. 2005, *ApJ*, 620, 984
- Jayawardhana, R. & Ivanov, V. D. 2006, *Science*, 313, 1279
- Jenkins, J. S., Pavlenko, Y. V., Ivanyuk, O., et al. 2012, *MNRAS*, 420, 3587
- Jordi, K., Grebel, E. K., & Ammon, K. 2006, *A&A*, 460, 339
- Kalas, P., Graham, J. R., Chiang, E., et al. 2008, *Science*, 322, 1345
- Kamiaka, S., Masuda, K., Xue, Y., et al. 2015, *PASJ*, 67, 94
- Kenyon, S. J. & Hartmann, L. 1995, *ApJS*, 101, 117
- Kirkpatrick, J. D., Dahn, C. C., Monet, D. G., et al. 2001, *AJ*, 121, 3235
- Kirkpatrick, J. D., Reid, I. N., Liebert, J., et al. 2000, *AJ*, 120, 447
- Koch, D. G., Borucki, W. J., Basri, G., et al. 2010, *ApJ*, 713, L79
- Koen, C. 2015, *MNRAS*, 450, 3991
- Konopacky, Q. M., Barman, T. S., Macintosh, B. A., & Marois, C. 2013, *Science*, 339, 1398
- Kraus, A. L. & Ireland, M. J. 2012, *ApJ*, 745, 5
- Kraus, A. L., Ireland, M. J., Cieza, L. A., et al. 2014, *ApJ*, 781, 20
- Kuzuhara, M., Tamura, M., Ishii, M., et al. 2011, *AJ*, 141, 119
- Kuzuhara, M., Tamura, M., Kudo, T., et al. 2013, *ApJ*, 774, 11
- Lafrenière, D., Jayawardhana, R., Janson, M., et al. 2011, *ApJ*, 730, 42
- Lafrenière, D., Jayawardhana, R., & van Kerkwijk, M. H. 2008, *ApJ*, 689, L153
- Lagrange, A.-M., Bonnefoy, M., Chauvin, G., et al. 2010, *Science*, 329, 57
- Lagrange, A.-M., Gratadour, D., Chauvin, G., et al. 2009, *A&A*, 493, L21
- Latham, D. W., Rowe, J. F., Quinn, S. N., et al. 2011, *ApJ*, 732, L24
- Lissauer, J. J., Jontof-Hutter, D., Rowe, J. F., et al. 2013, *ApJ*, 770, 131
- Liu, M. C., Magnier, E. A., Deacon, N. R., et al. 2013, *ApJ*, 777, L20
- Luhman, K. L., Adame, L., D'Alessio, P., et al. 2005a, *ApJ*, 635, L93
- Luhman, K. L., D'Alessio, P., Calvet, N., et al. 2005b, *ApJ*, 620, L51
- Luhman, K. L., Patten, B. M., Marengo, M., et al. 2007, *ApJ*, 654, 570
- Luhman, K. L., Wilson, J. C., Brandner, W., et al. 2006, *ApJ*, 649, 894
- Macintosh, B., Graham, J. R., Barman, T., et al. 2015, *Science*, 350, 64
- Mamajek, E. E. & Bell, C. P. M. 2014, *MNRAS*, 445, 2169
- Mannings, V. & Sargent, A. I. 1997, *ApJ*, 490, 792
- Mannucci, F., Basile, F., Poggianti, B. M., et al. 2001, *MNRAS*, 326, 745
- Marley, M. S. 2013, *Science*, 339, 1393
- Marley, M. S., Fortney, J. J., Hubickyj, O., Bodenheimer, P., & Lissauer, J. J. 2007, *ApJ*, 655, 541
- Marley, M. S., Saumon, D., Cushing, M., et al. 2012, *ApJ*, 754, 135
- Marois, C., Macintosh, B., Barman, T., et al. 2008, *Science*, 322, 1348
- Marois, C., Zuckerman, B., Konopacky, Q. M., Macintosh, B., & Barman, T. 2010, *Nature*, 468, 1080
- Martín, E. L., Zapatero Osorio, M. R., Barrado y Navascués, D., Béjar, V. J. S., & Rebolo, R. 2001, *ApJ*, 558, L117
- Mayor, M. & Queloz, D. 1995, *Nature*, 378, 355
- Metchev, S. A. & Hillenbrand, L. A. 2006, *ApJ*, 651, 1166
- Mohanty, S., Jayawardhana, R., Huélamo, N., & Mamajek, E. 2007, *ApJ*, 657, 1064
- Montet, B. T., Bowler, B. P., Shkolnik, E. L., et al. 2015, *ArXiv e-prints* [arXiv:1508.05945]
- Moya, A., Amado, P. J., Barrado, D., et al. 2010, *MNRAS*, 405, L81
- Muñoz, D. J., Kratter, K., Vogelsberger, M., Hernquist, L., & Springel, V. 2015, *MNRAS*, 446, 2010
- Mugrauer, M. & Neuhäuser, R. 2005, *Astronomische Nachrichten*, 326, 701
- Mugrauer, M., Vogt, N., Neuhäuser, R., & Schmidt, T. O. B. 2010, *A&A*, 523, L1
- Nagasawa, M. & Ida, S. 2011, *ApJ*, 742, 72
- Naud, M.-E., Artigau, É., Malo, L., et al. 2014, *ApJ*, 787, 5
- Neuhäuser, R., Errmann, R., Berndt, A., et al. 2011, *Astronomische Nachrichten*, 332, 547
- Neuhäuser, R., Errmann, R., Raetz, S., et al. 2013, in *Protostars and Planets VI Posters*, 47
- Neuhäuser, R., Guenther, E. W., Wuchterl, G., et al. 2005, *A&A*, 435, L13
- Neuhäuser, R. & Schmidt, T. O. B. 2012, *Topics in Adaptive Optics (InTech)*
- Ngo, H., Knutson, H. A., Hinkley, S., et al. 2015, *ApJ*, 800, 138
- Panić, O., Hogerheijde, M. R., Wilner, D., & Qi, C. 2009, *A&A*, 501, 269
- Patience, J., King, R. R., de Rosa, R. J., & Marois, C. 2010, *A&A*, 517, A76
- Peña Ramírez, K., Béjar, V. J. S., Zapatero Osorio, M. R., Petr-Gotzens, M. G., & Martín, E. L. 2012, *ApJ*, 754, 30
- Pecaut, M. J., Mamajek, E. E., & Bubar, E. J. 2012, *ApJ*, 746, 154
- Perryman, M. A. C. 2005, in *Astronomical Society of the Pacific Conference Series*, Vol. 338, *Astrometry in the Age of the Next Generation of Large Telescopes*, ed. P. K. Seidelmann & A. K. B. Monet, 3
- Pollack, J. B., Hubickyj, O., Bodenheimer, P., et al. 1996, *Icarus*, 124, 62
- Potter, D., Martín, E. L., Cushing, M. C., et al. 2002, *ApJ*, 567, L133
- Preibisch, T., Brown, A. G. A., Bridges, T., Guenther, E., & Zinnecker, H. 2002, *AJ*, 124, 404
- Quanz, S. P., Amara, A., Meyer, M. R., et al. 2015, *ApJ*, 807, 64
- Quanz, S. P., Amara, A., Meyer, M. R., et al. 2013, *ApJ*, 766, L1
- Rameau, J., Chauvin, G., Lagrange, A.-M., et al. 2013, *ApJ*, 772, L15
- Rasio, F. A. & Ford, E. B. 1996, *Science*, 274, 954
- Rayner, J. T., Cushing, M. C., & Vacca, W. D. 2009, *ApJS*, 185, 289
- Rebolo, R., Zapatero Osorio, M. R., Madrugá, S., et al. 1998, *Science*, 282, 1309
- Reid, I. N. & Walkowicz, L. M. 2006, *PASP*, 118, 671
- Reipurth, B. & Clarke, C. 2001, *AJ*, 122, 432
- Rieke, G. H. & Lebofsky, M. J. 1985, *ApJ*, 288, 618
- Safronov, V. S. & Zvjagina, E. V. 1969, *Icarus*, 10, 109
- Sallum, S., Follette, K. B., Eisner, J. A., et al. 2015, *Nature*, 527, 342
- Saumon, D. & Marley, M. S. 2008, *ApJ*, 689, 1327
- Schmidt, T. O. B., Mugrauer, M., Neuhäuser, R., et al. 2014, *A&A*, 566, A85
- Schmidt, T. O. B., Neuhäuser, R., Mugrauer, M., Bedalov, A., & Vogt, N. 2009, in *American Institute of Physics Conference Series*, Vol. 1094, 15th Cambridge Workshop on Cool Stars, Stellar Systems, and the Sun, ed. E. Sten- pels, 852–855
- Schmidt, T. O. B., Neuhäuser, R., Seifahrt, A., et al. 2008, *A&A*, 491, 311
- Schneider, J., Dedieu, C., Le Sidaner, P., Savalle, R., & Zolotukhin, I. 2011, *A&A*, 532, A79
- Siess, L., Dufour, E., & Forestini, M. 2000, *A&A*, 358, 593
- Skrutskie, M. F., Cutri, R. M., Stiening, R., et al. 2006, *AJ*, 131, 1163
- Sparks, W. B. & Ford, H. C. 2002, *ApJ*, 578, 543
- Spiegel, D. S. & Burrows, A. 2012, *ApJ*, 745, 174
- Stamatellos, D. & Whitworth, A. P. 2009, *MNRAS*, 392, 413
- Thatte, N., Abuter, R., Tecza, M., et al. 2007, *MNRAS*, 378, 1229
- Todorov, K., Luhman, K. L., & McLeod, K. K. 2010, *ApJ*, 714, L84
- van Eyken, J. C., Ciardi, D. R., von Braun, K., et al. 2012, *ApJ*, 755, 42
- Vorobyov, E. I. 2013, *A&A*, 552, A129
- Wahhaj, Z., Liu, M. C., Biller, B. A., et al. 2011, *ApJ*, 729, 139
- Weinberg, M. D., Shapiro, S. L., & Wasserman, I. 1987, *ApJ*, 312, 367
- Wright, J. T., Upadhyay, S., Marcy, G. W., et al. 2009, *ApJ*, 693, 1084
- Yu, L., Winn, J. N., Gillon, M., et al. 2015, *ApJ*, 812, 48
- Zacharias, N., Finch, C. T., Girard, T. M., et al. 2013, *AJ*, 145, 44
- Zacharias, N., Monet, D. G., Levine, S. E., et al. 2004, in *Bulletin of the American Astronomical Society*, Vol. 36, American Astronomical Society Meeting Abstracts, 1418
- Zapatero Osorio, M. R., Béjar, V. J. S., Martín, E. L., et al. 2000, *Science*, 290, 103
- Zuckerman, B., Rhee, J. H., Song, I., & Bessell, M. S. 2011, *ApJ*, 732, 61

Appendix A: Supplemental Material

CVSO 30 is currently not suitable for a common proper motion analysis (Table 1). As orbital motion around the host star might be detectable, we simulated the expected maximum separation (top) and position angle (bottom) change in Fig. A.1, dependent on inclination and eccentricity of the companion for an epoch difference of 3 years. This corresponds to our first astrometrically calibrated epoch from 2012 to a tentative new observation end of 2015. The dedicated orbital analysis shows that even after 2-3 years of epoch difference no significant orbital motion is expected for the wide companion.

A first spectrum of CVSO 30 c at an intermediate reduction step, shown in Fig. 3 (central panel), by subtracting an average spectrum of the spike, left and right of the companions psf from the superposition of companion and spike is given in Fig. A.2. We find the results before (red spectrum) and after (blue spectrum) spike subtraction, which also removes the still present OH lines. In addition the spectrum of the host star CVSO 30 is shown in black for comparison.

In Fig. A.3 we show the expected signal to noise ratio (S/N) for the given conditions and integration times (Tables 4 & 1) using ESO’s exposure time calculator for SINFONI and the latest available Pickles template spectrum M6 (blue). We derive the almost identical S/N using the flux of the companion after spike removal (Fig. 3) compared to the noise of the background next to the spike (black). However, these S/N estimates are not achieved for our final extracted spectrum and its noise estimate (Fig. 4), as the spike itself adds slight additional noise and more importantly because of the imperfect removal of the spike dominating the final S/N (red). To take this effect, likely caused by imperfect primary star positioning into account, we derived our final noise estimate, given as noise floor in Fig. 4, as standard deviation of the neighboring spectral channels after removal of the continuum at the spectral position of interest. This noise is also used for the spectral model fitting (Figs. 4 & 5) and the reduced χ^2 estimation for several comparison objects (Table 6).

We show the color-magnitude diagram given in Fig. 11 in the main document with the identification of all the unlabeled objects in a full version in Fig. A.5 with the corresponding references in Table A.2. The objects seem to follow the prediction of Saumon & Marley (2008) quite well, especially around 10 Myr. Only 2M1207 b seems to be far off, possibly because of an edge-on disk reddening the object heavily (Mohanty et al. 2007). Whether HR 8799 c, d are unusual can hardly be judged, as no similar object having very low luminosity is known at that age. HR 8799 b is, however, very low in luminosity (Fig. 9). The younger the objects the higher in luminosity they are at comparable spectral type because of their larger radius, since they are still experiencing gravitational contraction. The plot (Fig. A.5) implies that CVSO 30 c is the first very young (< 10 Myr) L-T transition object.

The core accretion model (Safronov & Zvjagina 1969; Goldreich & Ward 1973; Pollack et al. 1996), was also discussed in models for HR 8799 bcde by Close (2010), arguing that the inner planet was likely formed by core accretion, while for the outer ones the gravitational instability of the disk (Cameron 1978; Boss 1997) is the more probable formation scenario. However, HR 8799 is an A- or F-star, and recent numerical simulations (Vorobyov 2013) show that disk fragmentation fails to produce wide-orbit companions around stars with mass < 0.7 M_{\odot} , hence unfeasible for the $\sim 0.34 - 0.44 M_{\odot}$ M3 star CVSO 30. In addition the disk would have to be large enough for in situ formation. The most massive disks around M stars (e.g. IM Lupi) might be

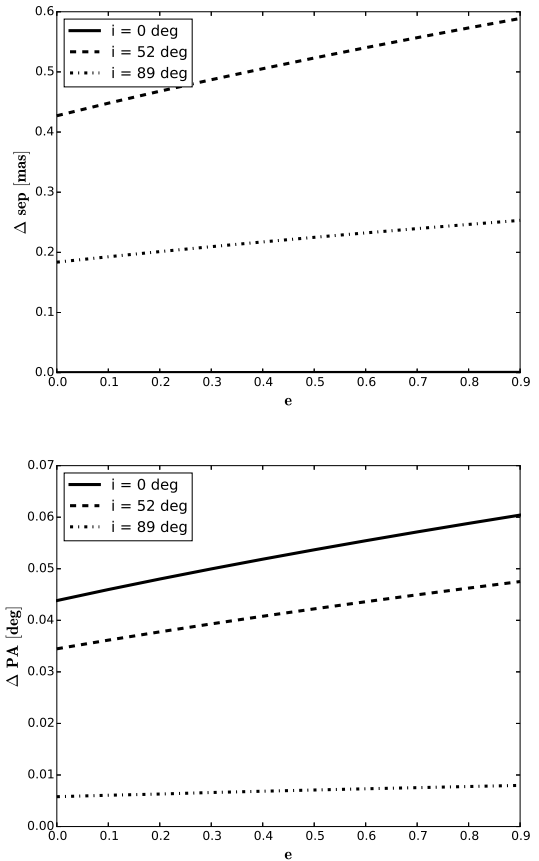


Fig. A.1. Expected maximum separation (top) and position angle (bottom) change, dependent on inclination and eccentricity of the companion for an epoch difference of 3 years (end of 2015, since first calibrated epoch was done end of 2012).

large enough, but in this case it was shown to possess almost all of its dust within 400 au separation (Panić et al. 2009), still too small for formation at 660 au.

If the object has not formed in situ, a very obvious solution would be scattering induced by a stellar flyby close to the system (Adams & Laughlin 2001; Muñoz et al. 2015) or with another object of the system. While Reipurth & Clarke (2001) describe this possibility for the formation of brown dwarfs by disintegration of a small multiple system and possibly a cutoff from the formation material reservoir, which might have happened e.g. for directly imaged circumbinary planet candidates, like ROSS 458(AB) c (Burgasser et al. 2010b) or SR 12 AB c (Kuzuhara et al. 2011) the even more obvious possibility would be planet-planet scattering as an inner planet candidate CVSO 30 b of comparable mass is present, that could have been scattered inward at the very same scattering event.

A way to discriminate between the formation scenarios would be by higher S/N ratio spectroscopy as done for HR 8799 c (Konopacky et al. 2013). With both H_2O and CO detected one is able to estimate the bulk atmospheric carbon-to-oxygen ratio and whether it differs from that of the primary star, which lead Marley (2013) to speculate that HR 8799 c formed by core accretion rather than gas instability.

We can put CVSO 30 c best into context by comparing with the recent M dwarf survey of Bowler et al. (2015), who find fewer than 6% of M dwarfs to harbor massive giant planets of 5–13 M_{Jup} at 10–100 au and that there is currently no statistical

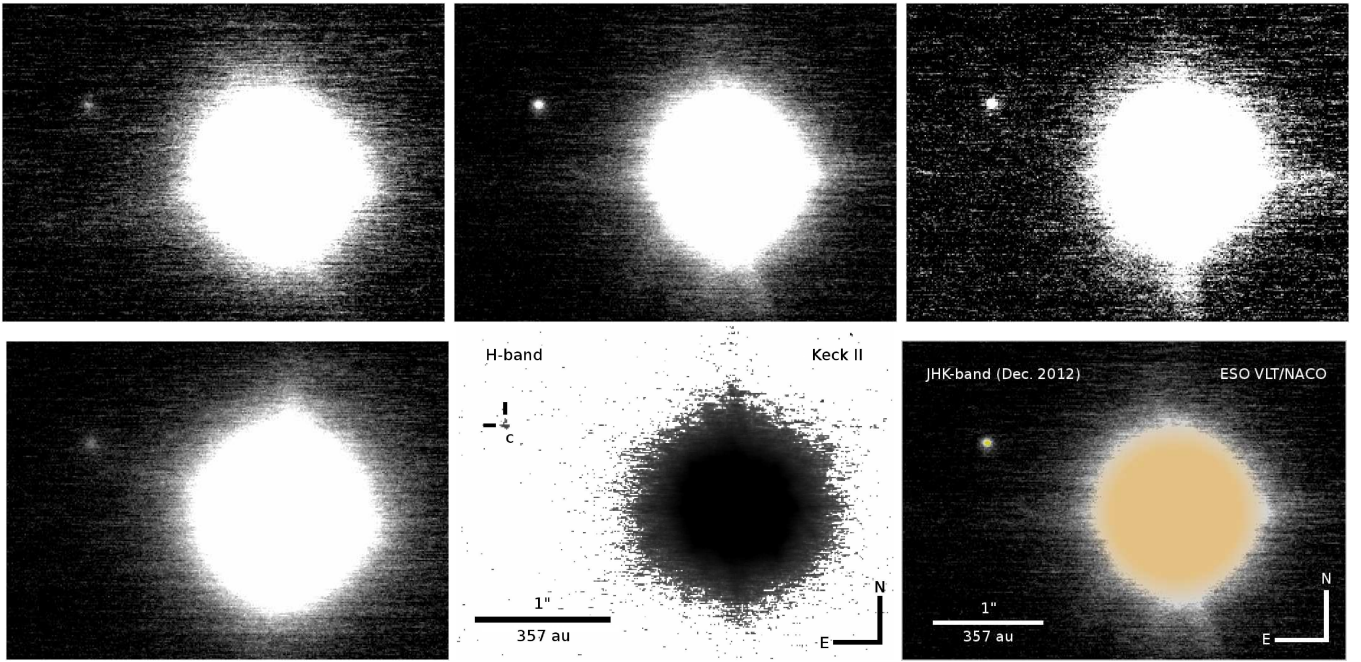


Fig. A.4. Direct Images of CVSO 30 c. *Top row, left to right:* Quasi-simultaneous VLT NACO J, H, Ks band data, taken in a sequence and shown in same percentage upper cut-off and lower cut-off value 0. *Lower row, left to right:* VLT NACO J band with double exposure time per single image, the same in total, Keck image of data by van Eyken et al. (2012), re-reduced, note, the companion is Northeast, not a contaminant Southeast as given in van Eyken et al. (2012) and a JHKs color composite, showing that CVSO 30 c has similar colors as its host star (Fig. 2).

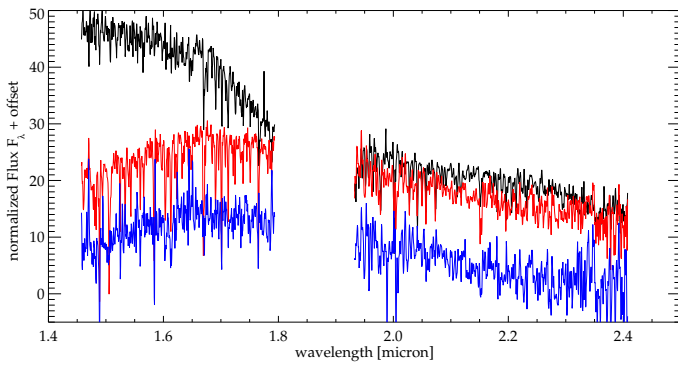


Fig. A.2. Spectrum of the primary (black) and the companion at the best illuminated pixel as given in the central panel of Fig. 3 (red; with OH lines). And the spectrum after subtraction of the average spike East and West of the companion (blue), composing about 30 % light contribution (beforehand). While the H-band spectrum presents a triangular shape and bluer color, indicating a young sub-stellar companion, the full continuum of the companion is not reliable as different amounts of flux is superimposed by the rotating primary spike, changing the overall continuum shape because of different spike removal quality.

evidence for a trend of giant planet frequency with stellar host mass at large separations. We note, however, that CVSO 30 c would probably not have been found at the distance of their targets, as it would not have been in the field of view, because of its large separation of about 660 au. About 20 of the 49 directly imaged planet candidates at www.exoplanet.eu have an M dwarf as host star.

At a projected separation of ~ 660 au, the system is above the long-term stability limit of ~ 390 au for a M3 primary star of $0.34 - 0.44 M_{\odot}$ (Table 1), following the argumentation of Weinberg et al. (1987) and Close et al. (2003). However, as shown in Mugrauer & Neuhauser (2005) 2M1207 and its companion

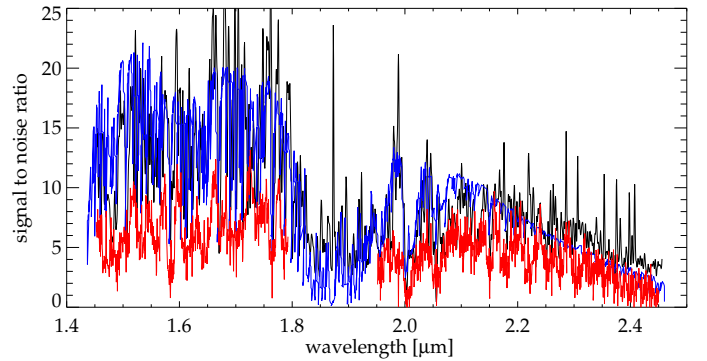


Fig. A.3. Signal to noise ratio (S/N) achieved for the brightest pixel vs. the background noise in the combined cube (black). For comparison the expected and almost identical S/N is shown, simulated using the exposure time calculator (ETC) of ESO/SINFONI (blue). In red we present the final achieved S/N of the extracted companion spectrum after removal of a superimposed spike (Fig. 3), as shown in Fig. 4.

(Chauvin et al. 2005a) are also exceeding this long-term stability limit at about three times the age of CVSO 30.

The currently acquired data is consistent with planet-planet scattering simulations in Ford & Rasio (2008), showing that massive planets are more likely to eject one another, whereas smaller planets are more likely to collide, resulting in stabilized systems, as supported by Kepler satellite and Doppler survey results finding predominantly smaller (Wright et al. 2009; Latham et al. 2011) low density (e.g. Lissauer et al. 2013) planets in compact close multiplanet systems.

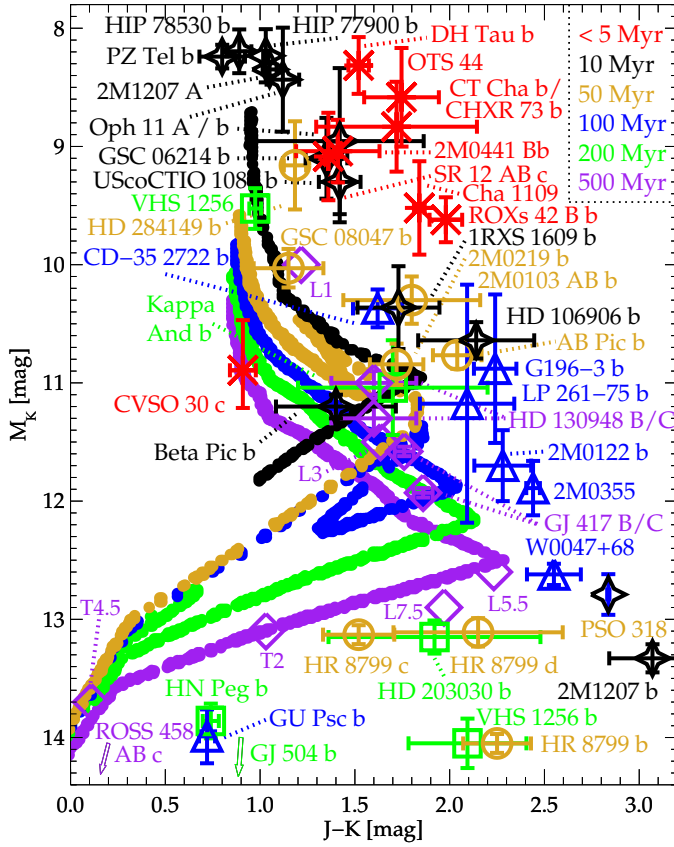


Fig. A.5. Color-magnitude diagram of simulated cluster brown dwarf population from Saumon & Marley (2008). Each sequence corresponds to a different age as given in the legend. Superimposed the position several planet candidates with full identification and CVSO 30 c. See Fig. 11 and Table A.2 for further details.

Table A.2. Color-magnitude plot (Figs. 11 & A.5) references

Object	reference	Object	reference
2M1207	Chauvin et al. (2004)	HR 8799	Marois et al. (2008)
A & b	Mohanty et al. (2007)	b, c, d	
b	Ducourant et al. (2008)	β Pic b	Bonnefoy et al. (2013)
1RXS	Lafrenière et al. (2008)	ROXs	Kraus et al. (2014)
1609 b		42B b	
DH Tau	Itoh et al. (2005)	SR 12	Kuzuhara et al. (2011)
b	Luhman et al. (2006)	AB c	
AB Pic	Chauvin et al. (2005c)	2M0103	Delorme et al. (2013)
b		AB b	
Ross	Burningham et al. (2011)	USco	Béjar et al. (2008)
458		CTIO	
AB c		108 b	
GSC	Ireland et al. (2011)	PZ Tel b	Mugrauer et al. (2010)
06214 b		GJ 504	Kuzuhara et al. (2013)
GU Psc	Naud et al. (2014)	b	
b		2M0122	Bowler et al. (2013)
HD	Metchev & Hillenbrand (2006)	b	
203030		HD	Potter et al. (2002)
b		130948	
GSC	Chauvin et al. (2005b)	B & C	
08047 b	Bonnefoy et al. (2014a)	2M0355	Faherty et al. (2013)
HN Peg	Luhman et al. (2007)	CD-35	Wahhaj et al. (2011)
b		2722 b	
κ And b	Carson et al. (2013)	OTS 44	Luhman et al. (2005b)
	Hinkley et al. (2013)	Cha	Luhman et al. (2005a)
HIP	Lafrenière et al. (2011)	1109	
78530 b		HD	Bonavita et al. (2014)
Oph 11	Jayawardhana & Ivanov (2006)	284149	
A & b	Close et al. (2007)	b	
LP	Reid & Walkowicz (2006)	HIP	Aller et al. (2013)
261-75	Kirkpatrick et al. (2000)	77900 b	
b		G196-3	Rebolo et al. (1998)
GJ 417	Kirkpatrick et al. (2001)	b	
B & C	Dupuy et al. (2014)	HD	Bailey et al. (2014)
CHXR	Luhman et al. (2006)	106906	
73 b		b	
CT Cha	Schmidt et al. (2008)	W0047	Gizis et al. (2015)
b		+68	
VHS	Gauza et al. (2015)	2M0219	Artigau et al. (2015)
1256 b		b	
2M0441	Bowler & Hillenbrand (2015)	PSO	Liu et al. (2013)
Bb		318	

Table A.1. Evolutionary plot (Fig. 9) references

Object	reference	Object	reference
GJ 504 b	Kuzuhara et al. (2013)	HD 95086	Rameau et al. (2013)
2M1207	Chauvin et al. (2004)	b	Galicher et al. (2014)
b	Mohanty et al. (2007)	HR 8799	Marois et al. (2008)
HR 8799	Marois et al. (2010)	b, c, d	Zuckerman et al. (2011)
e	Zuckerman et al. (2011)		Moya et al. (2010)
	Moya et al. (2010)	β Pic b	Lagrange et al. (2009)
1RXS	Lafrenière et al. (2008)		Bonnefoy et al. (2014b)
1609 b	Neuhäuser & Schmidt (2012)		Binks & Jeffries (2014)
	Pecaat et al. (2012)	CHXR 73	Mamajek & Bell (2014)
CT Cha b	Schmidt et al. (2008)	b	Luhman et al. (2006)
2M044	Todorov et al. (2010)	GQ Lup b	Neuhäuser et al. (2005)
144 b		LkCA15	Kraus & Ireland (2012)
HD	Quanz et al. (2013)	b, c	Sallum et al. (2015)
100546b	Quanz et al. (2015)	SR 12	Kuzuhara et al. (2011)
ROXs	Currie et al. (2014)	AB c	
42B b		2M0103	Delorme et al. (2013)
DH Tau	Itoh et al. (2005)	AB b	
b	Neuhäuser & Schmidt (2012)	HD	Bailey et al. (2014)
AB Pic b	Chauvin et al. (2005c)	106906 b	
	Neuhäuser & Schmidt (2012)	GU Psc b	Naud et al. (2014)
51 Eri b	Macintosh et al. (2015)		GSC
	Montet et al. (2015)	06214 b	Ireland et al. (2011)
USco	Béjar et al. (2008)	PZ Tel B	Preibisch et al. (2002)
CTIO	Preibisch et al. (2002)		Mugrauer et al. (2010)
108 b	Pecaat et al. (2012)		Billier et al. (2010)
2M0219 b	Artigau et al. (2015)		Jenkins et al. (2012)